Generating a link between a cell division and suicide gene provides a measure and solution for cell therapy safety

Generating a link between a cell division and suicide gene provides a measure and solution for cell therapy safety

Qin Liang[1, 2, *], Claudio Monetti[1, *], Maria V Shutova[1], Eric J Neely[1, 2], Sabiha Hacibekiroglu[1, 2], Huijuan Yang[1, 3], Christopher Kim[1. 2], Puzheng Zhang[1], Chengjin Li[1], Kristina Nagy[1,3] Maria Mileikovsky[1], Istvan Gyongy[4], Hoon-Ki Sung[1, 5] and Andras Nagy[1, 2, 6, 7]

[1] Lunenfeld-Tanenbaum Research Institute, Sinai Health System, Toronto, Canada
[2] Institute of Medical Science, University of Toronto, Toronto, Canada
[3] Department of Physiology, University of Toronto, Toronto, ON, Canada
[4] School of Mathematics and Maxwell Institute, The University of Edinburgh, Edinburgh, UK
[5] The Hospital for Sick Children Research Institute, Toronto, ON, Canada
[6] Australian Regenerative Medicine Institute, Monash University, Melbourne, VIC, Australia
[7] Department of Obstetrics & Gynaecology, University of Toronto, Toronto, ON, Canada
[*] These authors contributed equally to this work.

Running Title: Defining cell therapy safety

Text word count Summary paragraph: 158
Text word count main text: 3245
Number of Figures: 4
Methods word count: 3327
Number of Extended Data Figures: 10
Number of Supplementary Tables: 3
Number of Supplementary Video: 1
Number of Supplementary Calculation: 1

Keywords: cell therapy, defining cell therapy safety, fail-safe cell system, fail-safe level, pluripotent stem cells, therapeutic cells, tumorigenicity, mutation rate, cell division essential locus, suicide gene, genome editing, human, mouse

Corresponding author: Andras Nagy, nagy@lunenfeld.ca

The advent of human pluripotent cell lines holds enormous promise for the development of cell therapies to treat degenerative disease. Safety, however, is a crucial pre-condition for clinical application. Numerous groups have attempted to eliminate potentially harmful cells through the use of suicide genes[1]; however, none of these efforts quantitatively define safety. Here, we show a concept for the protection of a suicide transgene system from inactivation and its realisation with genome engineering strategies. The strategy behind our fail-safe (FS) design is to create a transcriptional link between the suicide gene herpes simplex virus-thymidine kinase (HSV-TK) and a cell division essential gene, Cyclin-Dependent Kinase 1 (*CDK1*). Furthermore, we add a quantitative measure to cell therapy safety as the function of the cell number needed for a therapy and the type of genome editing performed. Even with the highly conservative estimates described here, we anticipate that our solution and the quantification of safety will rapidly accelerate the entry of cell-based medicine to the clinic.

Most randomly integrated transgenes are not stably expressed in all cells. The transfected cell population will show variegated expression as a result of epigenetic and genetic modifications, developmental regulation, mutations, and/or complete loss of the transgene[2-4]. To alleviate these mechanisms, we generated a transcriptional link between a cell division essential locus (CDEL) and a drug-inducible suicide system (SU), resulting in a CDEL-SU allele (Fig. 1a). In this design, the expression of the CDEL and SU are tightly linked together, and if required, the dividing cells of a graft can be eliminated or arrested through treatment with the SU prodrug. With an SU placed in a CDEL essential for cell-life, the entire graft could be eliminated regardless of its proliferative status.

According to the engineering definition, fail-safe systems are designed to mitigate potential harm caused by a system failure. Using this terminology, a cell population is considered fail-safe if all of the cells within the population contain a functional SU. The fail-safe level (FSL) is defined as a number. It indicates that the odds of using a non-FS batch of cells for therapy is one out of this number (Fig. 1b), such as one out of a thousand (FSL=1,000) or one out of a million (FSL=1,000,000) batches. Here, we used various *in vitro* and *in vivo* experiments as well as mathematical modelling to define the FSL that needs to be satisfied for future cell therapies to be designated as safe.

To generate a list of CDEL candidates, we cross-referenced genes whose knock-out has an early embryonic lethal phenotype in mice (http://www.informatics.jax.org/phenotypes.shtml) with data from a genome-wide CRISPR/Cas9 mutagenesis screen for essential genes in human cancer cell lines[5]. We found 167 genes with a high-fitness score (< -1.0)[5] that also have a known early-embryonic lethal phenotype (Supplementary Table 1). For this study, we chose *CDK1* as our prototype CDEL and an optimised mutant version of HSV-TK, TK.007[6] (TK from now on), as the SU prototype. Genetic studies have shown that CDK1 is an essential kinase[7]. Its absence causes a block in the G2/M transition of the cell cycle, and other CDKs are not able to rescue its deficiency[8,9]. TK has been extensively used for cell ablation[10], and its mechanism of action in the presence of its clinically-approved prodrug ganciclovir (GCV), is well characterised[11]. Importantly, *CDK1* and the linked TK are not expressed in non-dividing cells[9], thus eliminating the potential immunogenicity of the viral TK protein[12] in quiescent donor cells.

To generate a transcriptional link between *CDK1* and TK (Fig. 1c), we used CRISPR/Cas9-assisted genome targeting to insert TK into the 3' untranslated region (3'UTR) of *CDK1* in mouse C2[13] (Extended Data Fig. 1a-d, 2a-c), human H1[14] (Extended Data Fig. 1e-i, 3a-f) and human CA1[15] (Extended Data Fig. 4a-e) embryonic stem (ES) cells. Next, we determined the optimal GCV concentration for the heterozygous *CDK1*-TK mouse and human ES cells *in vitro* (Extended Data Fig. 2d, 3h), and then subsequently tested if we could control the growth of teratomas generated from these lines. Subcutaneous grafting of mouse ES cells into isogenic C57BL/6N recipients, and human ES cells into immunodeficient NOD scid gamma (NSG) recipients, resulted in teratoma formation with the expected efficiency (Extended Data Fig. 2e, 3g, 4d). When the volume of these tumours reached 500 mm^3 (considered as day 0), we

administered GCV daily by intraperitoneal injection for up to four weeks. Exposure to GCV rendered the C2 ES cell-derived teratomas dormant, without any sign of growth rebound following the treatment (Fig. 1d, e and Extended Data Fig. 5a). The heterozygous H1 ES cell-derived teratomas in NSG mice responded similarly, albeit, in most of the cases, repeated and more extended GCV treatments were required to stabilise the teratoma size (Fig. 1f and Extended Data Fig. 5c). The observed decrease in teratoma size following GCV re-administration (Extended Data Fig. 5c) indicates that quiescent or slow-dividing cells within the teratoma began proliferating following drug withdrawal, and consequently, expressed TK and became sensitive to GCV. Furthermore, we found that the volume of the human teratomas frequently increased in the later phase of the experiments (Extended Data Fig. 5d); however, in agreement with previous reports[16,17], this increase was the result of extensive cyst formation (Extended Data Fig. 5d) and not solid tissue growth. The induced long-term dormancy of the teratomas was encouraging but also unexpected as we predicted that such a large ES cell-derived tissue (~10^9 cells[18]) would contain hundreds of cells capable of escaping the SU through different types of mutations, such as silencing mechanisms and loss-of-heterozygosity (LOH). Within the well-encapsulated teratoma, however, it is likely that these assumed resistant cells (escapees) were eliminated by the known bystander killing effect of the TK/GCV system[19].

To further investigate the capacity of the FS system to control cell proliferation, we also performed a breast cancer transplantation assay using heterozygous FS mammary epithelial tumour cells[20]. Upon transplantation in an isogenic setting, we observed that after a delayed period (~100 days) the heterozygous FS tumours became resistant to GCV and continued growing in the presence of the drug (Extended Data Fig. 6a,b).

To identify escapees appearing in the expansion of heterozygous FS ES cells, we designed an *in vitro* experiment to mitigate the bystander killing effect (Extended Data Fig. 7a,b) and subsequently characterised the resistance mechanism in the eight independent clonal escapee-lines we obtained from 120 million cells. To determine if the escapee-generating mechanism was due to large genomic changes or *Cdk1*-TK locus-specific, we analysed the copy number (CN) of *Cdk1*, the TK transgene, and six additional endogenous genes all located on chromosome 10 (Fig. 1i, Extended Data Fig. 7d). Interestingly, this analysis revealed that only one escapee (E3 in Fig. 1i) contained the TK gene (Extended Data Fig. 7c). Further analyses did not detect mutations in the coding region of either *Cdk1* or TK (data not shown) but found the expression level of this allele was compromised and rendered the cells GCV resistant (Extended Data Fig. 7e). Another escapee, E5, was the result of a regional deletion involving the *Cdk1*-TK locus, and this led to at least an 18.5 Mbp hemizygous region in the wild type chromosome (predicted by CN=1 in *Sim1*, *Rhobtb1*, *Cdk1* and *Ank3* genes (Fig. 1i, Extended Data Fig. 7d). Regarding the other six clones, the diploidy (CN=2) of all of the examined endogenous chromosome 10 genes and the lack (CN=0) of TK suggested that these six escapees were formed by diploid LOH (dLOH). This was likely due to mitotic recombination events or chromosomal non-disjunction which homozygosed the wild type *Cdk1* allele in a diploid form. In summary, our data indicate that dLOH is the dominant mechanism of losing the *Cdk1*-TK allele in heterozygous ES cells. This finding is consistent with a study of mouse *Aprt* heterozygous cells, where dLOH accounted for 78% of the observed loss of gene function events[21].

To mitigate the generation of escapees by dLOH, we established both mouse and human ES cells homozygous for the *CDK1*-TK allele (Extended Data Fig. 2a-c, 3a-h, 4a-e). As expected, we were unable to identify any escapees when we repeated the above experiment (Extended Data Fig. 7b). It was not surprising that the homozygous ES cell-derived teratomas behaved similarly to the heterozygous teratomas; a brief GCV treatment was sufficient to render these tissues dormant (Fig. 1g,h, Extended Data Fig. 5b,e). As observed for the human heterozygous lines, cyst formation also occurred in the human homozygous teratomas (Extended Data Fig. 5e). Furthermore, we also generated homozygous FS mammary tumour cells and, following transplantation, observed that the size of these tumors could be reduced and their growth restrained through GCV administration (Extended Data Fig. 6c). The observed

growth rebound following GCV withdrawal was not surprising as slow-dividing or quiescent, tumour-prone MMTV-PyMT cells survive GCV administration and can start growing in the absence of the drug. Nevertheless, even in this non-clinical, extreme situation where a tumour cell line is used for cell transplantation, the homozygous FS system is still capable of managing and controlling tumour growth. Since we were unable to identify any escapees appearing in homozygous FS ES cell expansion, we used Monte Carlo (MC) simulation to estimate the odds of generating an escapee in this scenario. The model considers three different types of mutations which could affect the function of the CDEL-SU link (Fig. 2a). Type 1 mutations (su1) render the SU non-functional while keeping the linked CDEL operational. Type 2 mutations (su2) eliminate both SU and CDEL functionality through epigenetic or genetic changes to the entire locus, including a hemizygous LOH-dependent mechanism. Type 3 mutations remove a functional CDEL-SU allele by dLOH.

To estimate the probabilities of the type 1, 2 and 3 mutations (p1, p2 and p3, respectively) per cell generation (Fig. 2a), we used our targeted human H1 *CDK1*-TK-mCherry/*CDK1*-TK-EGFP dichromatic cell line, as most mutations in either *CDK1*-TK allele result in monochromatic cells. We grew 21 parallel cultures from a single dichromatic cell to an average of $5x10^6$ cells per culture (> 22 consecutive doublings) and determined the number of monochromatic cells in the culture using flow cytometry. Next, we applied Luria-Delbruck fluctuation analysis[22,23] to calculate the sum of the p1+p2+p3 probabilities in the two *CDK1*-TK alleles. We found that the mutation rate of losing mCherry was $9.05x10^{-6}$ per cell per division while the mutation rate of losing EGFP was similar at $7.68x10^{-6}$ per cell per division (Extended Data Fig. 8a-b).

To further validate the probabilities of these various mutations, we also analysed published studies that focused on these events. In mouse ES cells, the mutation rate (p1+p2+p3) of changing from a dichromatic to a monochromatic phenotype in the *Rosa26* locus (mouse Chr. 6) was $1x10^{-5}$ per cell, per division[24]. Similarly, another study calculated the mutation rate of gene function loss in the *Gdf9* locus (mouse Chr. 11) to be $2.3x10^{-5}$ events per cell per division[25]. Furthermore, the probability of the type 3 mutation, p3 alone, has been calculated as $1x10^{-5}$, $7.2x10^{-6}$ and $8.5x10^{-6}$ in three different studies[26-28] by performing high G418 selection in mouse ES cells. The p1+p2 mutation rate has also been estimated in the human *HPRT* locus on the X chromosome to be $1.7\text{-}6x10^{-7}$ by Luria-Delbruck fluctuation analysis[29], and $5x10^{-6}$ through mutation frequency analysis in population datasets[30].

Next, we performed MC simulation to establish the FSL of cell batches derived from different SU genotypes. Based on both published data and our own, we used the values $p1=p2=10^{-6}$ and $p3=2x10^{-5}$ per cell per division; all of which are intentional overestimates. Consequently, our calculated FSLs represent underestimates, being equal or lower than the actual FSL.

In silico, we subsequently generated a sufficient number of cell batches that were expanded from a single cell with an intact SU system. In every doubling, the model permits allele transitions (Fig. 2b) which determine the transition graph (depicted in Fig. 2c); reflecting the genotype change that could occur during cell expansion. For the homozygous *CDK1*-TK/*CDK1*-TK simulation, we initiated the batch production from an SU/SU cell, while for the heterozygous *CDK1*-TK/$CDK1^{wt}$ simulation, the initiating cell was SU/su1. Lastly, for the compound heterozygous *CDK1*-TK/$CDK1^{null}$ simulation, the initiating cell was SU/su2, since the su1 is functionally equivalent to $CDK1^{wt}$, while su2 is the same as a $CDK1^{null}$ allele (Fig. 2a).

A batch of cells is considered FS if it does not contain any escapees (Fig. 2d). The MC simulation determined the frequency of getting a non-FS batch of cells, which allowed us to calculate the FSL as the function of the cell number needed for a therapeutic cell batch. Fig. 2e shows these functions for the different initiating cell genotypes detailed above.

The number of cells required for a cell therapy is disease-specific and is estimated to range between 10^5 (i.e. eye[31,32]) and 10^{10} (i.e. heart[33]) cells. The genotype scenarios presented in Fig. 2e shows that a single TK insertion (*CDK1*-TK/$CDK1^{wt}$, *CDK1*-TK/$CDK1^{null}$) gives a low FSL for the cell numbers

required for therapy. Contrarily, a homozygous TK insertion into *CDK1* significantly increases the FSL and brings the safety into a clinically relevant range for many future cell therapies. Diseases, such as arthritis, diabetes or myocardial infarction, however, require a larger number of therapeutic cells (10^8 to 10^{10} donor cells). In this range, even the homozygous CDEL-SU provided FSL is insufficient (FSL<10). For this disease category, we propose the homozygous modification of two different CDELs with suicide genes. In this scenario, our MC simulation showed an enormous increase in FSL (FSL>10^6 for all clinically relevant batch volumes, Fig. 2e).

We observed that the logarithm of FSL, as a function of the logarithm of the cell number, is a convex function. It is very close to a linear function when the FSL is above 10 and the cell number is in the clinically relevant range. Therefore, for an estimation of FSL, we applied linear regression to these segments (Fig. 2e). Interestingly, the slope of the two linear regressions (Fig. 2e) is very close to minus one (-0.99) and the y-intercepts of these lines were close to 9 and 16 for one and two CDEL modifications, respectively. Using these approximates, the calculation of FSLs becomes very simple, while remaining the desired underestimates (Fig. 2e):

For one CDEL: $FSL = 10^9/cn$, and for two CDELs: $FSL = 10^{16}/cn$, where *cn* is the cell number needed for a therapeutic cell batch.

Concerning the production of cells for a specific therapy, some are lost during differentiation or expansion. To account for this, the efficiency of cell production should be accurately estimated and the cell number needed to generate a therapeutic batch should be corrected accordingly.

In future autologous cell therapies, the generation of multiple therapeutic batches might not be necessary, and a single FS clone could be grown up to the number of cells required for therapy. On the other hand, if allogeneic cells are desired or HLA haplobanks[34] of human pluripotent cell lines will be operational, the generation of an off-the-shelf bank of cell batches would be advantageous. In this scenario, it would be more practical and economical to produce a large pool of cells which, following quality control (QC) analysis, could be aliquoted into therapeutic doses. Consequently, we calculated the effect of aliquoting on FSL using both mathematical (Supplementary Calculation 1) and Monte-Carlo modeling approaches. On the basis of our established *in silico* model (Fig. 2e), we simulated the process of escapee accumulation until the final pool size reached 2^{20} and 2^{27} cells. In both of these scenarios, we calculated escapee generation frequency distributions. Next, we randomly picked A aliquots from these pools and calculated the mean number of "bad" aliquots (containing one or more escapee) in each case. By dividing the overall number of aliquots A by the number of bad aliquots, we calculated the aliquot FSL (*FSLap*). The ratio between *FSLap* and the FSL of the cell population size $2^{20}/A$ or $2^{27}/A$ (*FSLa*), is shown in Fig. 2f (red and orange lines, respectively). To confirm the results of this approach, we also calculated the same ratio using only theoretical assessment, where the final equation is as follows (Fig. 2f, blue line):

$$\frac{FSL_{ap}}{FSL_a} \approx \frac{1}{A\left(1-\sum_{k=0}^{m-1} 2^{-k-1}\left(\frac{A-1}{A}\right)^{2^k}\right)}$$

where A is the number of aliquots generated from the pool of cells, and m is the integer part of the base 2 log of the aliquot size.

The decrease in FSL is largest when a small number of aliquots are used (Fig. 2f, blue line). Within a practical range of aliquots (100-500), the FSL of the batches remains almost constant, with the probability modeling slightly underestimating the FSL drop. Consequently, aliquoting results in an approximately five-fold decrease in FSL using both approaches. The difference between aliquoting from a 2^{20} (~10^6) vs. 2^{27} (~ 10^9) pool shows that the drop is moderately larger (Fig. 2f) when we generate aliquots from a pool size that is close to the edge of the linear part on the original FSL graph (Fig. 2e).

Following the generation of every cell batch or pool, a quality control (QC) needs to be performed to ensure that the originating cell was FS and consequently, the FSL calculation was correct. To

demonstrate the practicality of the QC process, we grew several batches of cells from a single, homozygous FS ES cell. At the early phase of expansion, we verified that both *CDK1*-TK alleles were expressed and intact in the batch-originating single cell using flow cytometry and through allele-specific PCR (Extended Data Fig. 9) and sequencing of the TK-coding region.

Both mouse and human ES cells with the homozygous modification of *CDK1* have normal ES cell morphology and self-renewing capacity in standard ES cell culture conditions (Fig. 3a,b). The cells differentiated into the three embryonic germ layers in teratomas (Fig. 3c,d). Furthermore, we generated chimeric mice from the *Cdk1*-TK heterozygous mouse ES cells, and after germline transmission, obtained viable heterozygous and then homozygous adult mice (Fig. 3e, Extended Data Fig. 6a). Homozygous FS H1 human ES cells express pluripotency markers (Fig. 3f), and were successfully differentiated into retinal pigmented epithelial (RPE) cells[35] (Fig. 3g-i), adipocytes, osteocytes, chondrocytes (Fig. 3j), definitive endoderm (Fig. 3k), pharyngeal pouch endoderm[36] (Fig. 3l) and beating cardiomyocytes (Supplementary Video 1). Additionally, using *in vitro* neural differentiation, we demonstrated the selective killing of dividing cells by the FS system. As expected, following a brief GCV treatment, all mitotically active cells were eliminated while non-diving cells were spared (Fig. 3m). This ability could represent a valuable safety measure prior to the transplantation of cells into a recipient.

Although we previously demonstrated the robustness of the FS system using a breast cancer transplantation assay, we also wanted to simulate a clinical cell transplantation scenario gone awry. To accomplish this, we subretinally injected a 3:1 mixture of human homozygous FS RPE cells and human homozygous FS ES cells (mCherry tagged) into the eyes of NSG mice. Among 4 injected eyes, we did not observe any cell growth from the ES cell component of the graft when GCV was administered 24 hours post-injection for a period of 28 days, as a preventative measure (Fig. 4a-b, Extended Data Fig. 10a-c). In contrast, cell growth was detectable in 6 eyes that received an initial PBS treatment (Fig. 4c, Extended Data Fig. 10e-i). Importantly, even when GCV administration is delayed three weeks post-injection and cell growth has already been detected, the homozygous FS system efficiently stopped the growing ES cell-derived component of the graft; only non-dividing cells remained (Fig. 4c, Extended Data Fig. 10g-i). This experiment illustrates the ability of the FS system to selectively eliminate proliferating cells after cell transplantation. Furthermore, neither the initial nor the delayed GCV treatment affected the RPE graft or the integrity of the surrounding retinal tissue (Fig. 4b,c, Extended Data Fig. 10).

No therapy is without risk. Understanding and quantifying the risks associated with cell-based therapies is critical for the clinical advancement of regenerative medicine. Without a measurable safety system, it remains a challenging ambition to develop cell therapies that can treat degenerative diseases with an acceptable level of safety. We have developed a genome-editing strategy that allows a fundamental definition of safety, as well as a quantification of the safety level as a function of the cell number needed for any given cell therapy.

After transcriptionally linking a cell suicide element to a cell division essential locus, we mathematically defined and quantified the safety of our FS system. These calculated risks are highly conservative, and represent an underestimate of the actual safety level of the system, as they were performed using worst-case scenarios. This is necessary because the cells required for therapies (100 thousand to 10 billion) will need to be grown *ex vivo*. These conditions entail serious risks compared to most *in vivo* settings, where functional immune cells constantly surveil and eliminate transformed cells[37]. Additionally, since the number of cells needed will necessitate a similar number of genome duplications, any possible mutation could arise. Some mutations, such as a dominant negative heterozygous P53 can lead to a growth advantage[38] that allows mutant cells to rapidly take over the entire population within a competitive culture environment. For these reasons, the safety of *in vitro*-generated therapeutic cells must be vigorously assessed.

The concept and genome-editing approach presented here not only addresses these concerns, but also allows one to define cell therapy safety in a quantitative way. We contend that the risks, as determined

through experimentation and calculation, are sufficiently low and that the FS system will become an indispensable component of prospective cell therapies. Moreover, our approach to assess and quantify the safety of cell-based therapies will be critical for informed decision making by the regulators, clinicians and patients who will advance the therapies that will transform modern medicine.

1. Li, W. & Xiang, A. P. Safeguarding clinical translation of pluripotent stem cells with suicide genes. *Organogenesis* **9,** 34–39 (2013).
2. Dobie, K. Variegated gene expression in mice. *Trends in Genetics* **13,** 127–130 (1997).
3. Yagyu, S., Hoyos, V., Del Bufalo, F. & Brenner, M. K. Multiple mechanisms determine the sensitivity of human-induced pluripotent stem cells to the inducible caspase-9 safety switch. *Mol Ther Methods Clin Dev* **3,** 16003–8 (2016).
4. Kotini, A. G., de Stanchina, E., Themeli, M., Sadelain, M. & Papapetrou, E. P. Escape Mutations, Ganciclovir Resistance, and Teratoma Formation in Human iPSCs Expressing an HSVtk Suicide Gene. *Mol Ther Nucleic Acids* **5,** e284 (2016).
5. Wang, T. *et al.* Identification and characterization of essential genes in the human genome. *Science* **350,** 1096–1101 (2015).
6. Preuß, E. *et al.* TK.007: A Novel, Codon-Optimized HSVtk(A168H) Mutant for Suicide Gene Therapy. *Human Gene Therapy* **21,** 929–941 (2010).
7. Diril, M. K. *et al.* Cyclin-dependent kinase 1 (Cdk1) is essential for cell division and suppression of DNA re-replication but not for liver regeneration. *Proceedings of the National Academy of Sciences* **109,** 3826–3831 (2012).
8. Santamaría, D. *et al.* Cdk1 is sufficient to drive the mammalian cell cycle. *Nature* **448,** 811–815 (2007).
9. Satyanarayana, A. *et al.* Genetic substitution of Cdk1 by Cdk2 leads to embryonic lethality and loss of meiotic function of Cdk2. *Development* **135,** 3389–3400 (2008).
10. Fillat, C., Carrio, M., Cascante, A. & Sangro, B. Suicide Gene Therapy Mediated by the Herpes Simplex Virus Thymidine Kinase Gene / Ganciclovir System: Fifteen Years of Application. *Current gene therapy* **3,** 13–26 (2003).
11. Tomicic, M. T., Thust, R. & Kaina, B. Ganciclovir-induced apoptosis in HSV-1 thymidine kinase expressing cells: critical role of DNA breaks, Bcl-2 decline and caspase-9 activation. *Oncogene* **21,** 2141–2153 (2002).
12. Berger, C., Flowers, M. E., Warren, E. H. & Riddell, S. R. Analysis of transgene-specific immune responses that limit the in vivo persistence of adoptively transferred HSV-TK-modified donor T cells after allogeneic hematopoietic cell transplantation. *Blood* **107,** 2294–2302 (2006).
13. Gertsenstein, M. *et al.* Efficient generation of germ line transmitting chimeras from C57BL/6N ES cells by aggregation with outbred host embryos. *PLoS ONE* **5,** e11260–e11260 (2010).
14. Thomson, J. A. *et al.* Embryonic stem cell lines derived from human blastocysts. *Science* **282,** 1145–1147 (1998).
15. Adewumi, O. *et al.* Characterization of human embryonic stem cell lines by the International Stem Cell Initiative. *Nature Biotechnology* **25,** 803–816 (2007).
16. Damjanov, I. & Andrews, P. W. Teratomas produced from human pluripotent stem cells xenografted into immunodeficient mice - a histopathology atlas. *Int. J. Dev. Biol.* **60,** 337–419 (2016).
17. Wu, S. M. & Hochedlinger, K. Harnessing the potential of induced pluripotent stem cells for regenerative medicine. *Nat. Cell Biol.* **13,** 497–505 (2011).
18. Bianconi, E. *et al.* An estimation of the number of cells in the human body. *Ann. Hum. Biol.* **40,** 463–471 (2013).

19. Mesnil, M. & Yamasaki, H. Bystander effect in herpes simplex virus-thymidine kinase/ganciclovir cancer gene therapy: role of gap-junctional intercellular communication. *Cancer Research* **60,** 3989–3999 (2000).
20. Guy, C. T., Cardiff, R. D. & Muller, W. J. Induction of mammary tumors by expression of polyomavirus middle T oncogene: a transgenic mouse model for metastatic disease. *Molecular and Cellular Biology* **12,** 954–961 (1992).
21. Cervantes, R. B., Stringer, J. R., Shao, C., Tischfield, J. A. & Stambrook, P. J. Embryonic stem cells and somatic cells differ in mutation frequency and type. *Proceedings of the National Academy of Sciences* **99,** 3586–3590 (2002).
22. Luria, S. E. & Delbrück, M. Mutations of Bacteria from Virus Sensitivity to Virus Resistance. *Genetics* **28,** 491–511 (1943).
23. Capizzi, R. L. & Jameson, J. W. A table for the estimation of the spontaneous mutation rate of cells in culture. *Mutat. Res.* **17,** 147–148 (1973).
24. Larson, J. S., Yin, M., Fischer, J. M., Stringer, S. L. & Stringer, J. R. Expression and loss of alleles in cultured mouse embryonic fibroblasts and stem cells carrying allelic fluorescent protein genes. *BMC Mol Biol* **7,** 36 (2006).
25. Luo, G. *et al.* Cancer predisposition caused by elevated mitotic recombination in Bloom mice. *Nat Genet* **26,** 424–429 (2000).
26. Mortensen, R. M., Conner, D. A., Chao, S., Geisterfer-Lowrance, A. A. & Seidman, J. G. Production of homozygous mutant ES cells with a single targeting construct. *Molecular and Cellular Biology* **12,** 2391–2395 (1992).
27. Koike, H. *et al.* Efficient biallelic mutagenesis with Cre/loxP-mediated inter-chromosomal recombination. *EMBO Rep.* **3,** 433–437 (2002).
28. Yusa, K., Horie, K., Kondoh, G., Kouno, M. & Maeda, Y. Genome-wide phenotype analysis in ES cells by regulated disruption of Bloom's syndrome gene. *Nature* (2004).
29. Monnat, R. J. Molecular analysis of spontaneous hypoxanthine phosphoribosyltransferase mutations in thioguanine-resistant HL-60 human leukemia cells. *Cancer Research* (1989).
30. Green, M. H. L., O'Neill, J. P. & Cole, J. Suggestions concerning the relationship between mutant frequency and mutation rate at the hprt locus in human peripheral T-lymphocytes. *Mutation Research/Environmental Mutagenesis and Related Subjects* **334,** 323–339 (1995).
31. Schwartz, S. D. *et al.* Human embryonic stem cell-derived retinal pigment epithelium in patients with age-related macular degeneration and Stargardt's macular dystrophy: follow-up of two open-label phase 1/2 studies. *The Lancet* **385,** 509–516 (2015).
32. Mandai, M. *et al.* Autologous Induced Stem-Cell-Derived Retinal Cells for Macular Degeneration. *N. Engl. J. Med.* **376,** 1038–1046 (2017).
33. Chong, J. J. H. *et al.* Human embryonic-stem-cell-derived cardiomyocytes regenerate non-human primate hearts. *Nature* **510,** 273–277 (2014).
34. Barry, J., Hyllner, J., Stacey, G., Taylor, C. J. & Turner, M. Setting Up a Haplobank: Issues and Solutions. *Curr Stem Cell Rep* **1,** 110–117 (2015).
35. Klimanskaya, I. *et al.* Derivation and Comparative Assessment of Retinal Pigment Epithelium from Human Embryonic Stem Cells Using Transcriptomics. *http://www.liebertpub.com.myaccess.library.utoronto.ca/clo* **6,** 217–245 (2004).
36. Sun, X. *et al.* Directed Differentiation of Human Embryonic Stem Cells into Thymic Epithelial Progenitor-like Cells Reconstitutes the Thymic Microenvironment In Vivo. *Stem Cell* **13,** 230–236 (2013).
37. Dunn, G. P., Bruce, A. T., Ikeda, H., Old, L. J. & Schreiber, R. D. Cancer immunoediting: from immunosurveillance to tumor escape. *Nature Immunology* **3,** 991–998 (2002).
38. Merkle, F. T. *et al.* Human pluripotent stem cells recurrently acquire and expand dominant

negative P53 mutations. *Nature* **545,** 229–233 (2017).

Supplementary Information is linked to the online version of the paper at www.nature.com/nature.

Acknowledgements We thank the TCP Transgenic Core and Marina Gertsenstein for mouse line derivation, Annie Bang for flow cytometry, the TCP Pathology Core and Ken Harpal for histology analysis, Malgosia Kownacka for providing MEFs, Molly S. Shoichet for HAMC and Nikolaos Mitrousis for Q-PCR primers. We are also grateful to Sergey Nurk for advice on Monte Carlo simulation, to Iacovos P. Michael, Peter D. Tonge, Balasz V. Varga, Chen He and Rana El-Rass for experimental advice and Jeffrey S. Harding, and Kathryn C. Davidson for their proof-reading of the manuscript, to JSH for artwork. This work was supported by the CIHR foundation scheme, Canadian Research Chair and Medicine by Design (University of Toronto) to AN.

Author Contributions Q.L. and C.M. designed and conducted most of the experiments, analysed the data, and wrote the manuscript. M.V.S. conducted the Monte Carlo simulations and analysed the data. I.G. performed the mathematical modelling. E.J.N. conducted experiments and wrote the manuscript. S.H. performed the eye experiment and analysed the data. H.Y., C.K., P.Z., C.L., K.N., M.M., H.S. conducted experiments. A.N. conceived and supervised the study, designed experiments, analysed the data and wrote the manuscript.

Author Information Reprints and permissions information is available at www.nature.com/reprints. A.N., C.M. and Q.L. are inventors on a patent application covering the FS technology (PCT/CA2016/050256). A.N. is the co-founder and shareholder of panCELLa Inc. C.M. is a senior scientist at panCELLa Inc. The other authors declare no competing interests. Correspondence and requests for materials should be addressed to A.N. (nagy@lunenfeld.ca).

Methods

Generation of targeting vectors. Targeting vectors were generated by DNA synthesis, molecular cloning, recombineering and the NEBuilder HiFi DNA Assembly Cloning Kit (New England Biolabs).

Generation of CRISPR/Cas9 vectors. pX330-U6-Chimeric_BB-CBh-hSpCas9 was a gift from Feng Zhang (Addgene plasmid # 42230)[39]. Guide sequences for CRISPR/Cas9 were analyzed using the online CRISPR design tool (http://crispr.mit.edu). Guide sequence for mouse *Cdk1* targeting: TAAGAAGATGTAGCCCTC. Guide sequence for human *CDK1* targeting: CTATCTGTTGACATAACATA.

Mouse ES cell culture. C57BL/6N C2 ES cells were grown at 37°C in 95% air 5% CO_2 on MEFs obtained from TgN(DR4)1Jae/J mice (http://jaxmice.jax.org/strain/003208.html) at all times except for one passage on gelatinized tissue culture plates prior to aggregation[40]. Two types of media were used: 1). FBS-DMEM ES cell medium for gene targeting consisted of high glucose DMEM supplemented with 15% FBS (previously shown to support germline chimera generation), 2 mM GlutaMAX, 1 mM Na Pyruvate, 0.1 mM non-essential amino acids (NEAA), 50 U/ml penicillin and streptomycin (all Thermo Fisher Scientific), 0.1 mM 2-mercaptoethanol (Sigma) and 1000 U/ml LIF prepared with LIF producing plasmid.[41] 2). KOSR+2i medium was used for 2-4 passages prior to the generation of ES cell chimeras[13]. KOSR+2a consisted of high glucose DMEM medium supplemented with 15%

KnockOut Serum Replacement (KOSR) (Thermo Fisher Scientific), 1 mM Na Pyruvate, 0.1 mM NEAA, 0.1 mM 2-mercaptoethanol, 2 mM GlutaMAX, 50 U/ml penicillin/streptomycin, 500 U/ml LIF, 5 mg/ml Insulin (Thermo Fisher Scientific), 1 μM of the mitogen-activated protein kinase inhibitor PD0325901 (StemGent) and 3 μM of the glycogen synthase kinase-3 inhibitor CHIR99021 (StemGent). Cells were fed daily and passaged when they reached a confluency of 70-80%. 0.05% Trypsin-EDTA (Thermo Fisher Scientific) was used for the passage of cells grown in FBS-DMEM and Accutase (STEMCELL Technologies) was used for cells grown in KOSR+2i medium.

Mouse ES cell targeting. 50,000 mouse C57BL/6N C2 ES cells were transfected with 2 μg DNA (Mouse Target Vector 1 or 2: 1.5 μg, CRISPR vector: 0.5 μg) by JetPrime transfection (Polyplus). The cells were selected for G418-resistance (160 μg/ml) starting 48h after transfection. Resistant clones were picked independently and replicated in 96-well plates for freezing and genotyping with PCRs. PCR-positive clones were expanded, frozen to multiple vials, and genotyped by Southern blotting.

Selection cassette excision in mouse ES cells. Correctly targeted ES cell clones were transfected with episomal-hyPBase (for Mouse Target Vector I) or pCAGGs-NLS-Cre-IRES-puromycin (for Mouse Target Vector II). 2-3 days following transfection, cells were trypsinized and plated clonally (1,000 - 2,000 cells per 10 cm plate). mCherry-positive clones were picked and transferred to 96-well plates independently and genotyped by PCR and Southern blotting to confirm the excision event. The junctions of the removal region were PCR-amplified, sequenced, and confirmed to be intact and without any frameshift mutations. GCV (Sigma) to test for TK activity was used at a final concentration of 1 μM.

Human ES cell culture. Human CA1 and H1 ES cells were cultured on Geltrex (Thermo Fisher Scientific) using mTeSR1 media (STEMCELL Technologies) containing 50 U/ml penicillin/streptomycin (Thermo Fisher Scientific). Cells were passaged using TryplE Express (Thermo Fisher Scientific) and were subsequently plated in mTeSR media containing 10 μM ROCK inhibitor (Selleckchem) for 24 hours.

Human ES cell targeting. For Human Targeting Vectors I & II, 6 million human ES cells were electroporated using Neon Transfection System (Thermo Fisher Scientific) with protocol 14 (pulse voltage: 1200 mV, pulse width: 20 ms, pulse number: 2) with 24 μg DNA (Target Vector: 18 μg, CRISPR vector: 6 μg). After transfection, cells were plated on four 10 cm plates. G418 selection at 30 μg/ml or puromycin selection at 0.75 μg/ml was initiated 48h after transfection. Independent colonies were picked to 96-well plates and each plate was duplicated for further growth and genotyping with PCR. PCR-positive clones were expanded, frozen to multiple vials, and genotyped with Southern blotting. For Human Target Vector III targeting, 10 million human ES cells were electroporated using Neon protocol 14 with 40 μg DNA (Human Target Vector III: 30 μg, CRISPR vector: 10 μg), and plated in four 10 cm plates. 3-4 days after transfection, cells that were double-positive for mCherry and eGFP were sorted into one well of a 96-well plate. After recovery from FACS, cells were dissociated and plated clonally (1,000 - 2,000 cells per 10 cm plate). Next, clones were picked independently, replicated, and transferred to 96-well plates for freezing and genotyping with PCR. PCR-positive clones were expanded, frozen to multiple vials, and genotyped by Southern blotting.

Selection cassette excision in human ES cells. 1 million correctly targeted ES cell clones were electroporated with 2 μg episomal-hyPBase-IRES-puro (for Human Target Vector I) or 2 μg episomal-Cre-IRES-puro (for Human Target Vector II) using Neon protocol 14. Once the cells were confluent in 6-well plates, mCherry-positive cells were sorted to one well of a 96-well plate by FACS. After recovery, cells were dissociated and plated clonally (1,000 - 2,000 cells per 10 cm plate). Clones were

picked and transferred to 96-well plates independently and genotyped by PCR and Southern blotting to confirm the excision event. The junctions of the removal region were PCR-amplified, sequenced and confirmed to be intact and without frameshift mutations.

PCR genotyping. 2X Taq PCR master mix (Biomart) was used for all PCR reactions. Genomic DNA from human cell pellets was extracted using the DNeasy Blood & Tissue Kit (Qiagen). The primer pairs and conditions used for each reaction are listed in Supplementary Table 2.

Southern blotting. 10 μg of genomic DNA was extracted from PCR-positive clones, digested with ScaI-HF overnight, resolved by 0.6 - 0.7% gel electrophoresis, and transferred to Hybond N+ (GE Healthcare). The following probes were labelled with ^{32}P and used to hybridize with the membrane (~25 ng probe per ml hybridization solution). Human *CDK1* genomic probe: PCR amplified with primers h*CDK1*-Probe6-F + h*CDK1*-Probe6-R. Mouse *Cdk1* genomic probe: PCR amplified with primers 647302FWD + 647302REV. mCherry probe: the entire length of mCherry. eGFP probe: the entire length of eGFP. TK-mCherry probe: cut from h*CDK1*-PB-neo-TK-mCherry with Bsu36I+SgrAI: 1092 bp, gel-purified.

Mice. The CD-1 (ICR) (Charles River) outbred albino stock was used as embryo donors for aggregation with ES cells and as pseudopregnant recipients. C57BL/6NCrl (Charles River) was used as the host for teratoma assays with mouse C2 ES cells. C57BL/6NCrl or B6N-Tyr_c N4/Crl#493 (Charles River) was used as the host for mammary fat pad transplantation of mammary epithelial cells. NOD scid gamma /J#5557 (Jackson Laboratories) was used as the host for teratoma assays with human H1 or CA1 ES cells. FVB/N-Tg(MMTV-PyVT)634Mul/J was a gift from Dr. William Muller's lab[20], and the backcross to B6J background was done by Dr. Anthony Pawson's lab. Animals were maintained on a 12 h light/dark cycle and provided with food and water *ad libitum* in individually ventilated units (Techniplast) in the specific-pathogen free facility at The Centre for Phenogenomics (TCP). All procedures involving animals were performed in compliance with the Animals for Research Act of Ontario and the Guidelines of the Canadian Council on Animal Care.

Generation of chimeras and mouse lines. Morula aggregations were performed as previously described[40]. Chimeras were identified at birth by the presence of black eyes and later by coat pigmentation. Male chimeras with more than 50% ES cell contribution to coat colour were bred with CD-1 females to identify germline transmitter. The transmitter was then bred with C57BL/6NCrl females and pups were confirmed by genotyping to obtain *Cdk1*-TK/*Cdk1* mice. *Cdk1*-TK/*Cdk1* MMTV-PyMT males were generated by breeding MMTV-PyMT (B6) males and *Cdk1*-TK/*Cdk1* females. *Cdk1*-TK/*Cdk1*; MMTV-PyMT and *Cdk1*-TK/*Cdk1*-TK; MMTV-PyMT female mice were generated by breeding *Cdk1*-TK/*Cdk1*; MMTV-PyMT males and *Cdk1*-TK/*Cdk1* females.

Teratoma assay. Matrigel Matrix High Concentration (Corning) was diluted 1:3 with cold DMEM media on ice. 1-5 million mouse ES cells or 5-10 million human ES cells were suspended in 100 μl of Matrigel-DMEM and injected subcutaneously into one or both dorsal flanks of C57BL/6NCrl mice (for mouse C2 ES cells) and NOD scid gamma /J#5557 mice (for human H1 and CA1 ES cells). Teratomas formed 2-4 weeks after injection. Teratoma size was measured using calipers and volume was calculated using the formula V= (LxWxH)π/6. GCV /PBS treatment was performed through daily intraperitoneal injections (50 mg/kg) with varying treatment durations. At the end of treatment, mice were sacrificed and tumors were dissected and fixed in 4% paraformaldehyde for histological analysis.

Breast cancer transplantation assay. *Cdk1*-TK/*Cdk1*; MMTV-PyMT and *Cdk1*-TK/*Cdk1*-TK; MMTV-PyMT female mice developed mammary gland tumours between 3-6 months old. Mammary epithelial tumorigenic cells were isolated from developed tumours through digestion in 10× collagenase/hyaluronidase (STEMCELL Technologies), and dilution to 1x with media consisting of DMEM/F12 (Thermo Fisher Scientific) + 10% FBS + 50 U/ml penicillin/streptomycin for an hour in 37 degree. The digested cells were washed and pelleted with DMEM/F12 + 10% FBS 4 times, and plated in CnT-PRIME epithelium culture media (CELLnTEC Advanced Cell Systems AG) on plates coated with 0.1% gelatin (Sigma). Without passaging, primary mammary epithelial cells were dissociated and re-suspended in PBS at 10,000 cells per µl, and 50 µl (500,000 cells) was transplanted to each mouse by intraductal injection after making a small abdominal skin incision as previously described[42]. Tumour measurement and PBS/GCV treatment were the same as described in the teratoma assay.

Differentiation of human ES cells into retinal pigmented epithelial (RPE) cells. RPE differentiation was performed as previously described[35] with minor changes. Human ES cells were plated on Geltrex-coated 6-well plates and cultured in feeder-free conditions with mTeSR medium until confluency was reached and the colonies lost their tight borders (7-10 days). Next, the media was replaced with differentiation media (basal media with 13% KOSR) and changed every 2-3 days. The basal media consisted of KO-DMEM supplemented with 50 U/ml penicillin/streptomycin mix, 1 mM Na Pyruvate, 0.1 mM NEAA, 2 mM of GlutaMAX and 0.1 mM 2-mercaptoethanol. Initial pigmentation was observed approximately 3 weeks after the switch to differentiation media. Clusters of RPE cells were manually picked and transferred to a Geltrex-coated 24-well plate (3 clusters/well) when they were large enough (~1mm in diameter) for enrichment and the media was changed to RPE media, consisting of basal media with 5% FBS, 7% KSR and 10 ng/ml bFGF (Peprotech).

Differentiation of human ES cells into definitive endoderm. Definitive endoderm differentiation was performed using the STEMdiff Trilineage Differentiation Kit (StemCell Technologies), and characterized by immunostaining for SOX17 and FOXA2 (Supplementary Table 3).

Differentiation of human ES cells into pharyngeal pouch endoderm (PPE). PPE differentiation was performed as previously described[36] with the only modification being that the induction from ES cells to definitive endoderm is one day shorter than reported.

Differentiation of human ES cells into mesenchymal stem cells (MSCs) and subsequent adipogenic, osteogenic and chondrogenic differentiation. ES cells were cultured in mTeSR medium for 2 days. Next, cells were induced into early mesoderm progenitor cells with STEMdiffMesenchymal Induction Medium (STEMCELL Technologies) for 4 days and then were maintained with MesenCult-ACF Medium (STEMCELL Technologies). Cells were continually passaged onto 6-well plates pre-coated with MesenCult-ACF Attachment Substrate (STEMCELL Technologies) to derive early mesenchymal progenitor cells. At day 21, the MSCs showed a fibroblast-like morphology and the culture medium was changed every 3 days. For adipogenic differentiation, MSCs at a density of 20,000 cells/well were plated with MesenCult-ACF Attachment Substrate and cultured with MesenCult-ACF Medium for 2 days. Adipogenesis was induced using the StemPro Adipogenesis Differentiation Kit (Thermo Fisher Scientific). After 21 days, lipid droplets were visualized using Oil Red O (Sigma). For osteogenic differentiation, ES-derived MSCs at the density of 50,000 cells/well were plated with MesenCult-ACF Attachment Substrate and cultured with MesenCult-ACF Medium for 2 days. Osteogenesis was induced using the StemPro Osteogenesis Differentiation Kit (Thermo Fisher Scientific). After 21 days, calcium deposition was visualized using Alizarin Red (Sigma). For induction of chondrogenic differentiation, ES-derived MSCs were centrifuged in 15 ml conical tubes at 500g for

5 mins to create cell pellets with 5,000,000 cells per pellet. Chondrogenesis was induced using the StemPro Chondrogenesis Differentiation Kit (Thermo Fisher Scientific). After 21 days, cartilage was visualized using Alcian Blue (Sigma). Differentiation media was changed every 3 days.

Differentiation of human ES cells into beating cardiomyocytes. Cardiomyocyte differentiation was performed using STEMdiff Cardiomyocyte Differentiation Kit (STEMCELL Technologies).

Differentiation of human ES cells into neuronal progenitors and neurons. To differentiate human ES cells into neuronal progenitors, human ES cells were plated at 50-100,000 cells per cm^2 in 1:1 DMEM/F12 : Neurobasal (Thermo Fisher Scientific), 0.5x N2 supplement (home-made, 1.92 mg/ml putrescine, 2.376 µg/mL progesterone, 3.6 µM Selenium, 10 mg/mL Apo-transferrin, 0.75% BSA, 20 g/ml insulin), 0.5x B27 supplement with Vitamin A (Thermo Fisher Scientific), 2 mM Glutamax, 0.1 mM Beta-mercaptoethanol, 50 U/ml penicillin/streptomycin, 10 µM SB431542 (Selleckchem), 100 nM LDN193189 (Selleckchem) (+10 µM ROCK inhibitor overnight only, then removed). Cells were maintained in this condition for 8 days and media was changed every other day. Next, neuronal progenitors were dissociated with Accutase and plated at a density of $5x10^4$ cells per cm^2 on laminin (Sigma, 1 µl for $1cm^2$, diluted in 250 µl PBS without Ca and Mg) in fast neuron differentiation media, 1:1 DMEM-F12: Neurobasal, 1x B27 supplement with Vitamin A, 5 µM DAPT (Selleckchem), 2 mM Glutamax, 0.1 mM Beta-mercaptoethanol, 50 U/ml penicillin/streptomycin. Media were changed every three days. 10 µM GCV was added 6 days after neuron differentiation and kept for 6 days. 10 µM BrdU (Sigma) was added after 5 days of GCV treatment and the cultures were fixed after 6 days of GCV treatment and were immunostained for BrdU and beta-TublinIII (Supplementary Table 3).

Flow cytometry analysis and fluorescence-activated cell sorting (FACS). Flow cytometry and FACS were both performed and analyzed by the Lunenfeld-Tanenbaum Research Institute flow cytometry facility. FACS was performed using the ASTRIOS EQ cell sorter. Flow cytometry was performed using the GALLIOS flow cytometer and evaluated using Kaluza Analysis Software (Beckman Coulter). Samples were gated for live single cells using forward scatter, side scatter and DAPI staining. Wild-type and single-color samples of the same cell type as the experimental samples were used for negative controls and compensation calculations. Human ES cell samples were single-cell sorted using StemFlex Medium (Thermo Fisher Scientific) plus 10 µM ROCK inhibitor.

Immunostaining. 4% PFA-fixed cells were blocked and permeabilized with 5% goat serum + 1M Glycine + 1% Triton X-100 (all Sigma) in PBS without Ca and Mg or animal-free blocker (Vector Laboratories) + 1% Triton X-100 in milliQ water. All of the primary antibody information can be found in Supplementary Table 3. Staining was visualized using a Zeiss LSM780 confocal microscope.

Histology analysis. Paraffin embedding, paraffin block sectioning, and H&E staining were performed by the Pathology Core of The Centre for Phenogenomics.

Quantitative PCR. Gene expression analyses were completed as follows: RNA extraction by GenElute™ Mammalian Total RNA Miniprep Kit (Sigma), reverse transcription with QuantiTect Reverse Transcription Kit (Qiagen), Q-PCR with SensiFAST SYBR No-Rox Kit (Bioline) on Bio-Rad CFX Real-Time Systems (Bio-Rad), and analysis with Bio-Rad CFX Manager 3.1. All the information of primers and probes for the TaqMan Q-PCRs can be found in Supplementary Table 2. The reactions were performed using TaqMan Genotyping Master Mix (Thermo Fisher Scientific) and CFX Real-Time Systems, and were analyzed by CopyCaller Software v2.1 (Thermo Fisher Scientific).

Luria and Delbruck assay. The Luria and Delbruck assay was performed as previously described[22]. *CDK1*-TK homozygous 3C cells were single-cell plated in a 96-well plate using FACS. 21 single cell-derived cultures were grown to an average of 5 million cells per culture, and the number of single-positive cells in each culture were analyzed using flow cytometry. The mutation rate was calculated using the previously described equation[23] in https://www.wolframalpha.com/.

***In vivo* transplantation of RPEs.** *CDK1*-TK homozygous 3C ES cells were transfected with PB-CAGGs-mCherry-pA plasmid and sorted for high expressors. 40,000 3C-derived RPEs only or 30,000 3C-RPEs plus 10,000 mCherry-tagged 3C ES cells were injected subretinally with 0.5%/0.5% (wt/vol) hydrogel blend of hyaluronan and methylcellulose (HAMC) in HBSS. PBS or GCV (50 mg/kg) treatment were started the day after cell injection and were given every other day through intraperitoneal injections. Monitoring by fundoscopy and optical coherence tomography were performed on the day after transplantation and then once a week.

Monte Carlo simulation. An ES cell population was considered as a mix of mutant and non-mutant cells with reference to the CDEL-SU locus (or loci). All possible mutations were categorized into three different types: type 1, when only the SU part of the locus becomes non-functional (su1 allele); type 2, when both the CDEL and SU become non-functional (su2 allele); type 3, when any of the above occurs as a result of LOH (Fig. 2a,b). Back mutations, such as su1—>SU or su2—>SU or su2—>su1, were not considered, due to their extremely low probabilities (Fig. 2c). Back mutations, like SU/su1 -> SU/SU, SU/su2 -> SU/SU and su1/su2 -> su1/su1, were considered as a part of the more frequent LOH process. p1, p2, and p3 were designated the probabilities of each mutation type, respectively. We distinguished between two types of p3: p3mr (probability LOH occurred through mitotic recombination), where both daughter cells survive; and p3cnd (probability LOH occurred through chromosomal non-disjunction), where one of the daughter cells with the single remaining copy of the chromosome is likely to die[43]. On the basis of these probabilities, matrices of transitions between all possible genotypes within one or two CDEL systems were constructed (Fig. 2c, https://github.com/mashutova/failsafe).

With each division cycle (d), all cells within the population except cells with the su2/su2 genotype, were allowed to divide. Genotypes of su1/su2 and su1/su1 were considered escapees and the simulation initiated from one non-mutant cell. N(g1,d) was the number of cells of genotype g1 at doubling d, and p(g1,g2) was the probability of transition from genotype g1 to g2. In each doubling the number of cells changing genotype from g1 to g2 was determined through random sampling from a binomial distribution with parameters 2*N(g1,d-1) and p(g1,g2). We used Poisson approximation of binomial distribution to work with ultra-low p(g1,g2). For each division, the number of cells of each genotype was assessed, and the simulation proceeded until the first escapee was detected.

For each starting genotype, we performed more than 10 million simulations and obtained a distribution of the number of doublings from the detection of the first escapee. On the basis of this data, we generated a function of FSL (overall number of trials divided by number of trials with escapees) over cell population size (2^d) (Fig. 2d). Since all graphs contain almost linear regions, we used linear models to extrapolate them to high FSL values. To obtain linear regression lines, we only used simulated points from the linear-like part of the graph (R-squared > 0.999) with 95% confidence intervals less than 1000. To obtain a conservative boundary for the FSL, we used only the lowest CI values to build linear regressions.

To analyse the outcome from the aliquoting of the pool of fail-safe cells possibly containing escapees, using probability modelling we developed the following formula to calculate the drop of FSL (for details see Supplementary Calculation 1)

$$\frac{FSL_{ap}}{FSL_a} \approx \frac{1}{A(1-\sum_{k=0}^{m-1} 2^{-k-1}(\frac{A-1}{A})^{2^k})}$$

To reduce the complexity of the model, we considered only one escapee event in the pool, as the possibility of two independent escapees occurring in a pool is low in the quasi linear phase of FSL. Nevertheless, we tested the effect of this omission on the drop of FSL due to aliquoting using Monte Carlo simulation. We performed 10 million independent trials for a doubling of 20 and a doubling of 27, and obtained a distribution of the number of escapees for each of them. Through randomly sampling a number of escapees from each trial to the A aliquots, we calculated the number of "bad" aliquots containing one or more escapees (Ab). To calculate a new FSL of the population after aliquoting, where FSLp is the FSL of the original population, we used the formula A*FSLp/mean(Ab). The drop in FSL was measured *in silico* and was compared with the one we obtained from the equation obtained from the probability model.

Data availability. The DNA sequences of the vectors and plasmids used in this study are available upon request.

39. Cong, L. *et al.* Multiplex Genome Engineering Using CRISPR/Cas Systems. *Science* **339,** 819–823 (2013).
40. Behringer, R., Gertsenstein, M., Nagy, K. V. & Nagy, A. *Manipulating the Mouse Embryo*. (2013).
41. Mereau, A., Grey, L., Piquet-Pellorce, C. & Heath, J. K. Characterization of a binding protein for leukemia inhibitory factor localized in extracellular matrix. *The Journal of Cell Biology* **122,** 713–719 (1993).
42. Park, J., Kusminski, C. M., Chua, S. C. & Scherer, P. E. Leptin Receptor Signaling Supports Cancer Cell Metabolism through Suppression of Mitochondrial Respiration in Vivo. *The American Journal of Pathology* **177,** 3133–3144 (2010).
43. Biancotti, J.-C. *et al.* The in vitro survival of human monosomies and trisomies as embryonic stem cells. *Stem Cell Research* **9,** 218–224 (2012).

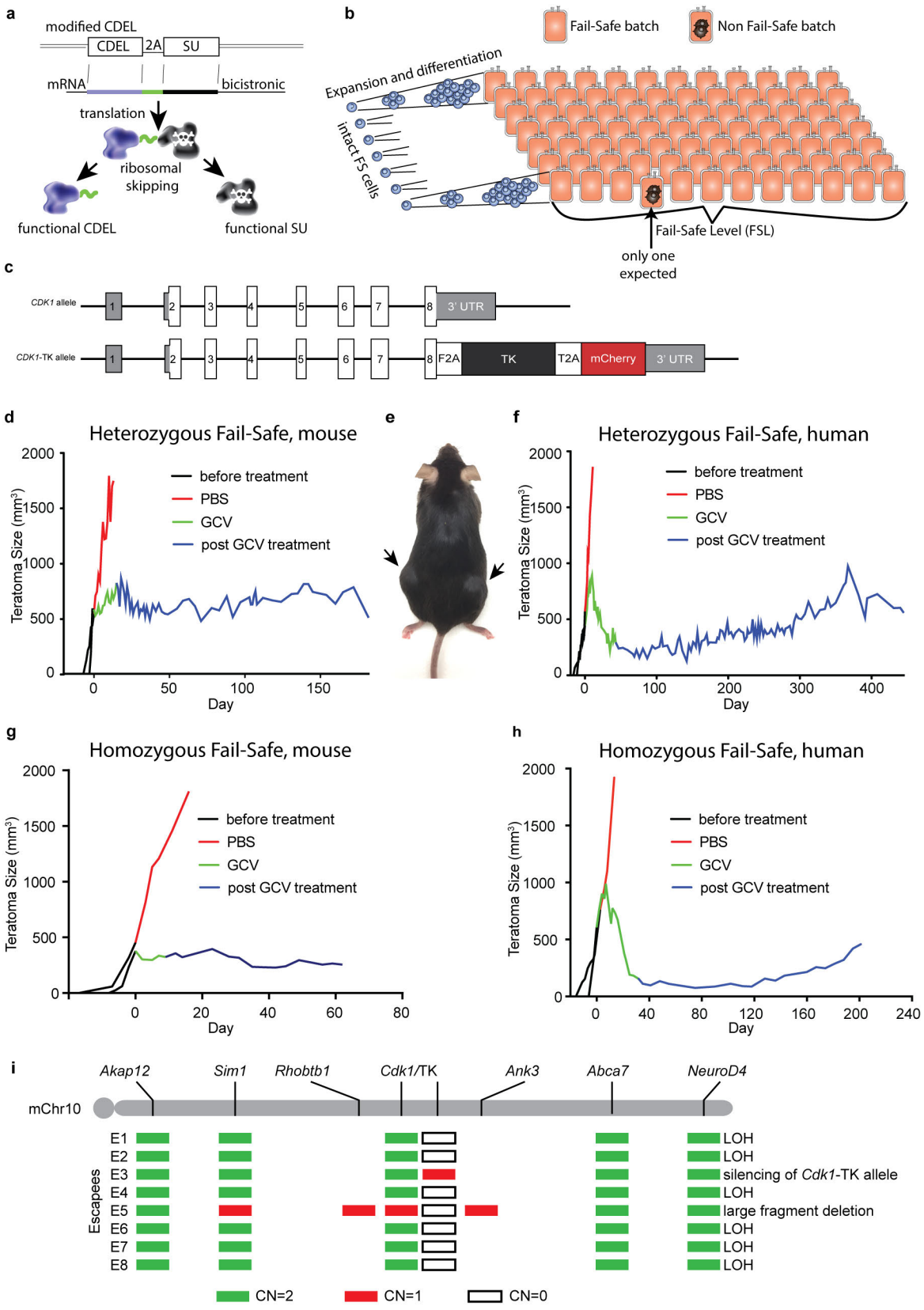

Figure 1 | Fail-safe cell system: the concept, the definition, realization and properties. a, The suicide gene is placed into a cell division essential locus (CDEL) resulting in a bicistronic mRNA that is translated into two proteins; a cell division essential factor and a drug-inducible suicide factor. **b**, Visual

representation of the fail-safe level (FSL) defined by one non-fail-safe batch out of how many batches. **c**, The link between the prototype SU (HSV-TK) and the prototype CDEL (*CDK1*). **d**, Representative growth of teratomas formed by mouse *Cdk1*-TK/*Cdk1* cells, when the recipients were treated with PBS or GCV. **e**, Adult mouse with stabilized subcutaneous tissue (fail-safe ES cell-derived dormant teratoma) 2.5 months after GCV treatment. **f**, Representative growth of teratomas formed by human *CDK1*-TK/*CDK1* ES cells, when the recipients were treated with PBS or GCV. **g,** Representative growth of teratomas formed by mouse *Cdk1*-TK/*Cdk1*-TK ES cells. **h,** Representative growth of teratomas formed by human *CDK1*-TK/*CDK1*-TK ES cells **i**, Copy number analysis of mouse *Cdk1*-TK/*Cdk1* escapees identified in the experiment described in Extended Data Fig. 7.

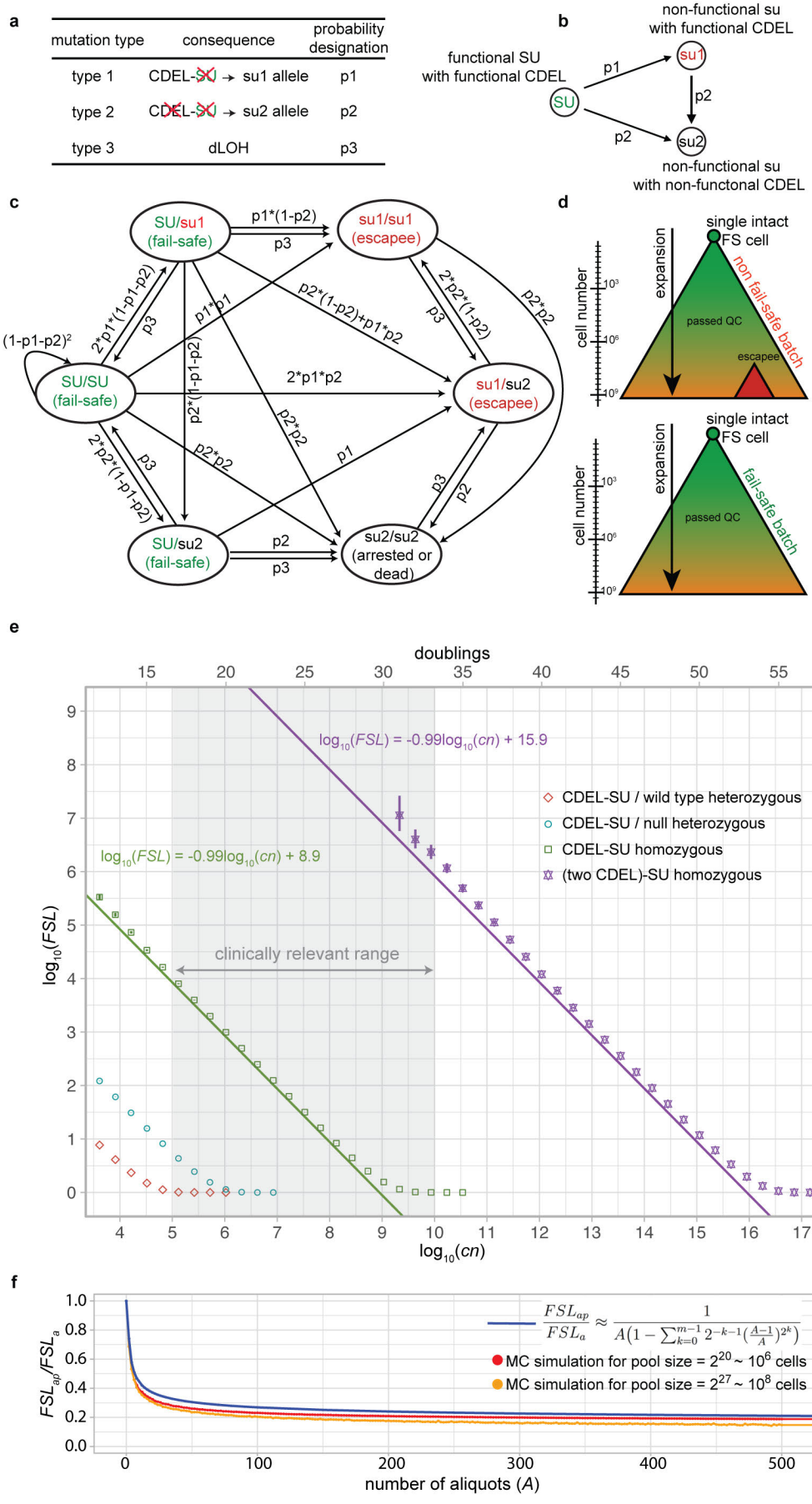
a
mutation type
consequence
probability designation
type 1
CDEL-SU → su1 allele
p1
type 2
CDEL-SU → su2 allele
p2
type 3
dLOH
p3
b
non-functional su with functional CDEL
functional SU with functional CDEL
SU
su1
su2
p1
p2
p2
non-functional su with non-functonal CDEL
c
SU/su1 (fail-safe)
su1/su1 (escapee)
SU/SU (fail-safe)
su1/su2 (escapee)
SU/su2 (fail-safe)
su2/su2 (arrested or dead)
(1-p1-p2)²
2*p1*(1-p1-p2)
p1*(1-p2)
p2*(1-p2)+p1*p2
2*p2*(1-p2)
p2*p2
p1*p1
2*p1*p2
p2*(1-p1-p2)
p1
d
single intact FS cell
expansion
cell number
passed QC
escapee
non fail-safe batch
fail-safe batch
e
doublings
log10(FSL) = -0.99log10(cn) + 15.9
log10(FSL) = -0.99log10(cn) + 8.9
CDEL-SU / wild type heterozygous
CDEL-SU / null heterozygous
CDEL-SU homozygous
(two CDEL)-SU homozygous
clinically relevant range
log10(FSL)
log10(cn)
f
FSLap/FSLa
MC simulation for pool size = 2^20 ~ 10^6 cells
MC simulation for pool size = 2^27 ~ 10^8 cells
number of aliquots (A)

Figure 2 | Modelling the FS cell system and calculating FSL. a, Three types of mutations that could affect the CDEL-SU allele. **b**, FS allele transition considered in the modelling and MC simulations. **c**, Genotype transition matrix considered in the modelling and MC simulations. **d**, Visual illustration of FS and non-FS batch formation during cell expansion. **e**, The function between therapeutic cell number and FSL determined by MC simulation (data points) for different initiating cell genotypes. Solid lines show the approximated linear regression on the "close to linear" part of the functions. The bars on certain data points represent the 95% confidence intervals of the FSL estimates. **f**, The drop of FSL due to aliquoting from a pool of cells relative to non-aliquoted batches of the same size.

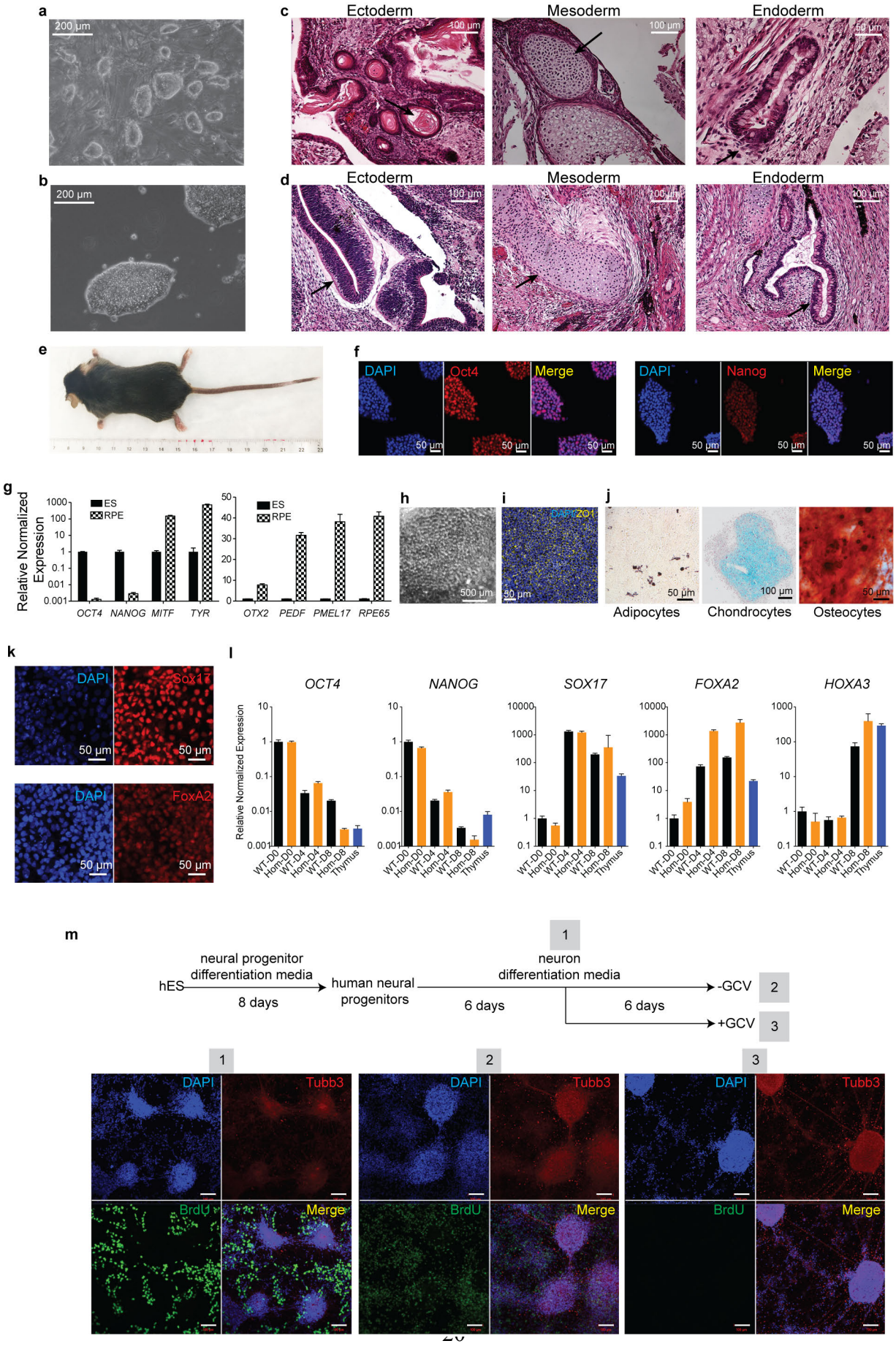
a
200 μm
b
200 μm
c
Ectoderm
Mesoderm
Endoderm
100 μm
d
Ectoderm
Mesoderm
Endoderm
100 μm
e
f
DAPI
Oct4
Merge
DAPI
Nanog
Merge
50 μm
g
Relative Normalized Expression
ES
RPE
OCT4
NANOG
MITF
TYR
OTX2
PEDF
PMEL17
RPE65
h
500 μm
i
DAPI ZO1
50 μm
j
Adipocytes
Chondrocytes
Osteocytes
k
DAPI
Sox17
FoxA2
50 μm
l
OCT4
NANOG
SOX17
FOXA2
HOXA3
Relative Normalized Expression
WT-D0
Hom-D0
WT-D4
Hom-D4
WT-D8
Hom-D8
Thymus
m
hES
neural progenitor differentiation media
8 days
human neural progenitors
1
neuron differentiation media
6 days
6 days
-GCV
2
+GCV
3
DAPI
Tubb3
BrdU
Merge

Figure 3 | Mouse and human fail-safe homozygous *CDK1*-TK/*CDK1*-TK cells demonstrate pluripotency. All experiments were performed using the same clone of mouse C2 or human H1 (Exc16-3C) *CDK1*-TK/*CDK1*-TK cells. **a**, Bright-field photograph showing mouse homozygous *Cdk1*-TK/*Cdk1*-TK ES cell morphology. **b**, Bright-field photograph showing human homozygous *CDK1*-TK/*CDK1*-TK ES cell morphology. **c**, H&E staining of a mouse *Cdk1*-TK/*Cdk1*-TK ES cell derived teratoma. **d**, H&E staining of a human *CDK1*-TK/*CDK1*-TK ES cell derived teratoma. **e**, An adult *Cdk1*-TK/*Cdk1*-TK mouse. **f**, OCT4 and NANOG staining of human *CDK1*-TK/*CDK1*-TK ES cells. **g**, Q-PCR characterization of *CDK1*-TK/*CDK1*-TK ES cell differentiation into RPE cells. Values represent mean ± SD, n = 3. **h**, Bright-field picture of human *CDK1*-TK/*CDK1*-TK ES cell derived RPE cells. **i**, ZO1 staining of human *CDK1*-TK/*CDK1*-TK ES cell derived RPE cells. **j**, Human *CDK1*-TK/*CDK1*-TK ES cell derived adipocytes, chondrocytes and osteocytes. **k,** SOX17 and FOXA2 staining of human *CDK1*-TK/*CDK1*-TK ES cell derived definitive endoderm. **l,** *OCT4*, *NANOG*, *SOX17*, *FOXA2* and *HOXA3* Q-PCR characterization of ES cell (Day 0) differentiation into definitive endoderm (Day 4) and pharyngeal pouch endoderm (Day 8). Values represent mean ± SD, n = 3. **m,** Human *CDK1*-TK/*CDK1*-TK ES cell differentiation into neural epithelial progenitors and subsequent neurons, with or without GCV treatment. Scale bar 100 μm.

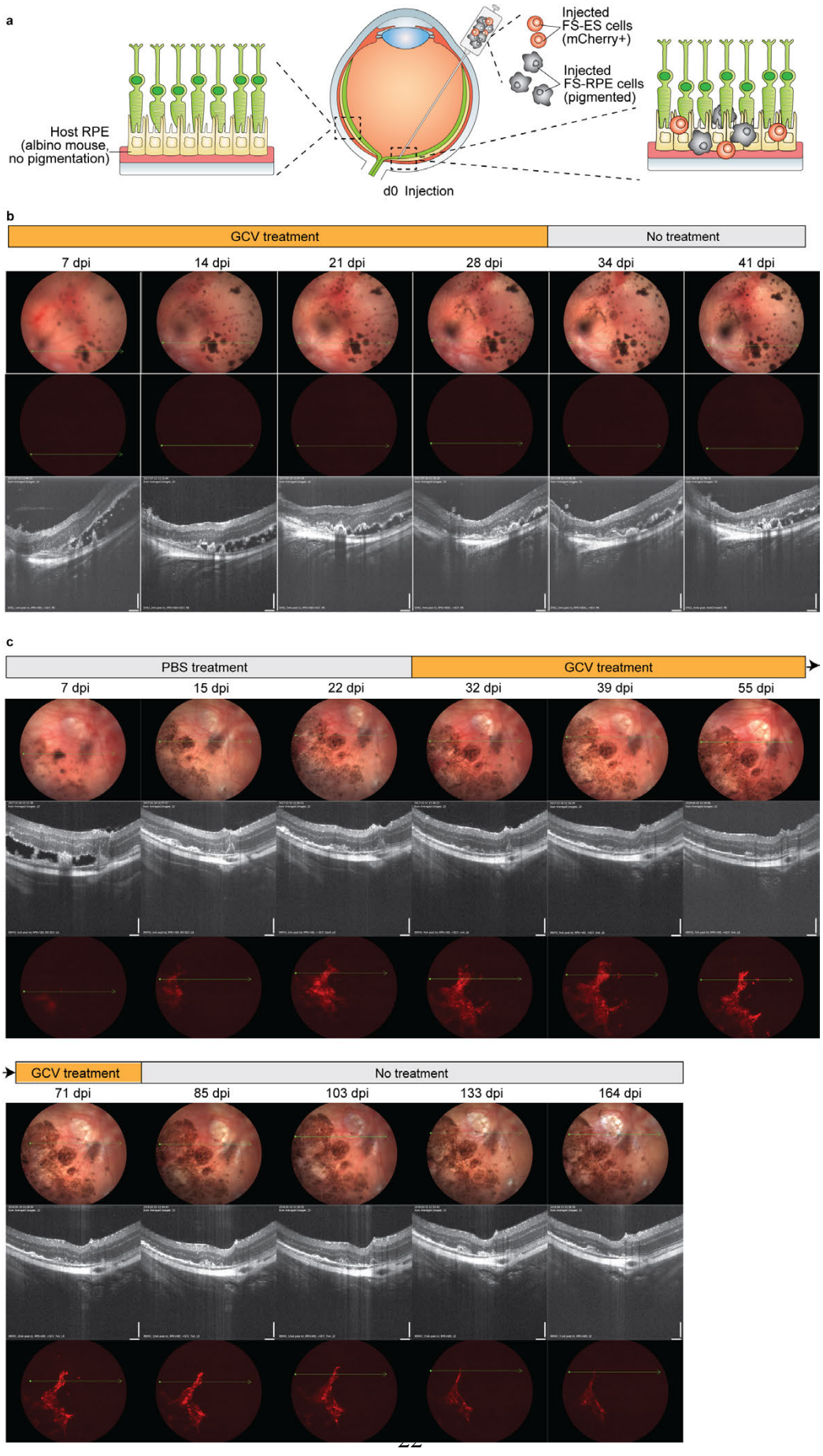
a
Injected
FS-ES cells
(mCherry+)
Injected
FS-RPE cells
(pigmented)
Host RPE
(albino mouse,
no pigmentation)
d0 Injection
b
GCV treatment
No treatment
7 dpi
14 dpi
21 dpi
28 dpi
34 dpi
41 dpi
c
PBS treatment
GCV treatment
7 dpi
15 dpi
22 dpi
32 dpi
39 dpi
55 dpi
GCV treatment
No treatment
71 dpi
85 dpi
103 dpi
133 dpi
164 dpi

Figure 4 | Fail-safe cell system in action; an *in vivo* proof of principle study. a, A 3:1 mixture of human homozygous FS ES cell-derived RPE cells and homozygous FS ES cells were subretinally co-injected into NSG mice and imaged using fundoscopy and optical coherence tomography (OCT) throughout GCV or PBS treatment. **b**, Fundoscopy, OCT and fluorescence imaging of the eye receiving GCV treatment (4 weeks). **c**, Fundoscopy, OCT and fluorescence imaging of the eye of the mouse that received PBS treatment (3 weeks) and developed an actively growing ES cell-derived lesion (mCherry+ cells). dpi stands for days post injection.

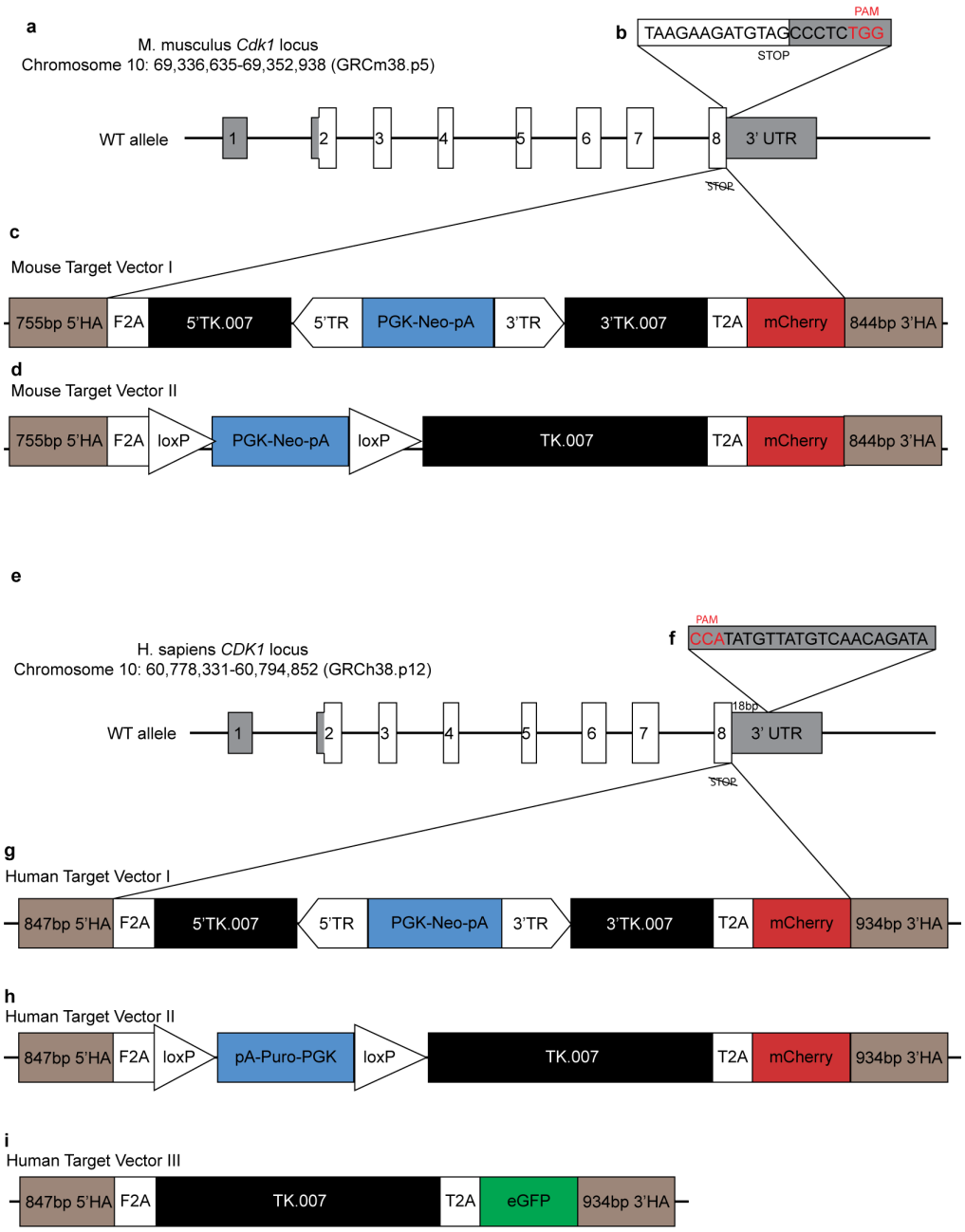

Extended Data Figure 1 | Schematic of targeting vectors for mouse and human *CDK1*. **a**, **e**, The genomic locus and structure of the mouse (**a**) and human (**e**) *CDK1* gene. **b**, **f**, CRISPR/Cas9 target site for mouse (**b**) and human (**f**) *CDK1*. **c**, **d**, **g**, **h**, **i**, The targeting vectors used in the study. The knock-in insertion replaced the *CDK1* stop codon with an F2A sequence, followed by the TK.007 linked to a fluorescent protein gene with a T2A sequence. Adding fluorescent reporters (mCherry and eGFP) to the insert permitted the visualisation of the modified *CDK1* allele expression in the cells. A positive selectable marker (neomycin or puromycin) was used to select for integration, and was subsequently removed by transiently expressing Cre recombinase or piggyBac (PB) transposase in the targeted cells, depending on the flanking loxP or PB terminal repeats (TR) in the target vector type, respectively. UTR: untranslated region, HA: homology arm, PGK: phosphoglycerate kinase, eGFP: enhanced green fluorescent protein, mCherry: mCherry fluorescent protein, pA: polyadenylation, Neo: neomycin selectable marker, Puro: puromycin selectable marker.

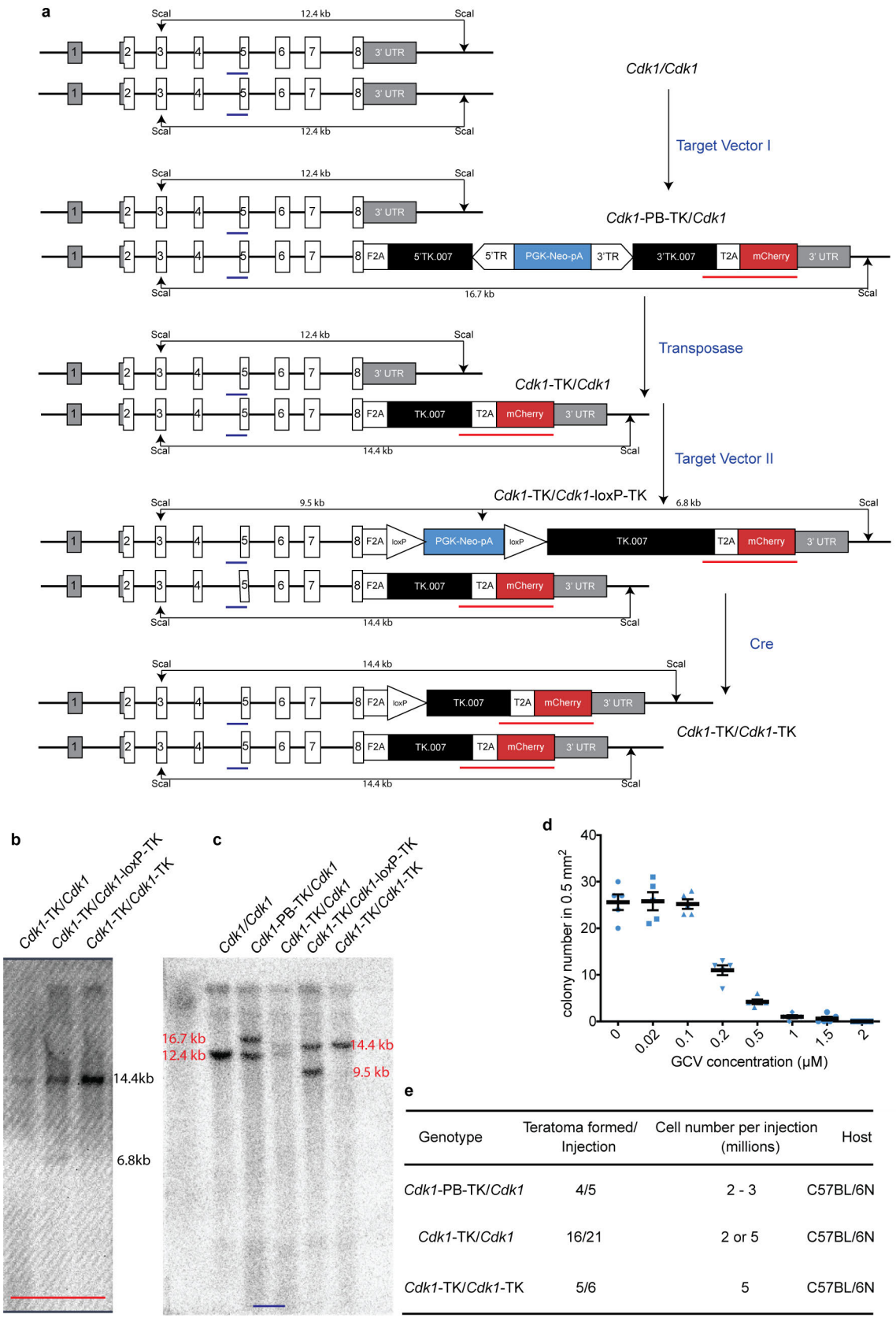

e

Genotype	Teratoma formed/ Injection	Cell number per injection (millions)	Host
Cdk1-PB-TK/*Cdk1*	4/5	2 - 3	C57BL/6N
Cdk1-TK/*Cdk1*	16/21	2 or 5	C57BL/6N
Cdk1-TK/*Cdk1*-TK	5/6	5	C57BL/6N

Extended Data Figure 2 | Generation, genotyping and characterization of mouse C57BL/6N C2 *Cdk1*-TK/*Cdk1* and *Cdk1*-TK/*Cdk1*-TK ES cells. a, Summary of the targeting steps used to generate

mouse C2 *Cdk1*-TK/*Cdk1* and *Cdk1*-TK/*Cdk1*-TK ES cells. **b**, Southern blot genotyping with internal TK-mCherry probe. **c**, Southern blot genotyping with mouse *Cdk1* genomic probe. **d**, *In vitro* GCV dose-response killing curve of mouse C2 *Cdk1*-TK/*Cdk1* ES cells. **e**, Teratoma formation efficiency of mouse C2 *Cdk1*-PB-TK/*Cdk1, Cdk1*-TK/*Cdk1* and *Cdk1*-TK/*Cdk1*-TK ES cells.

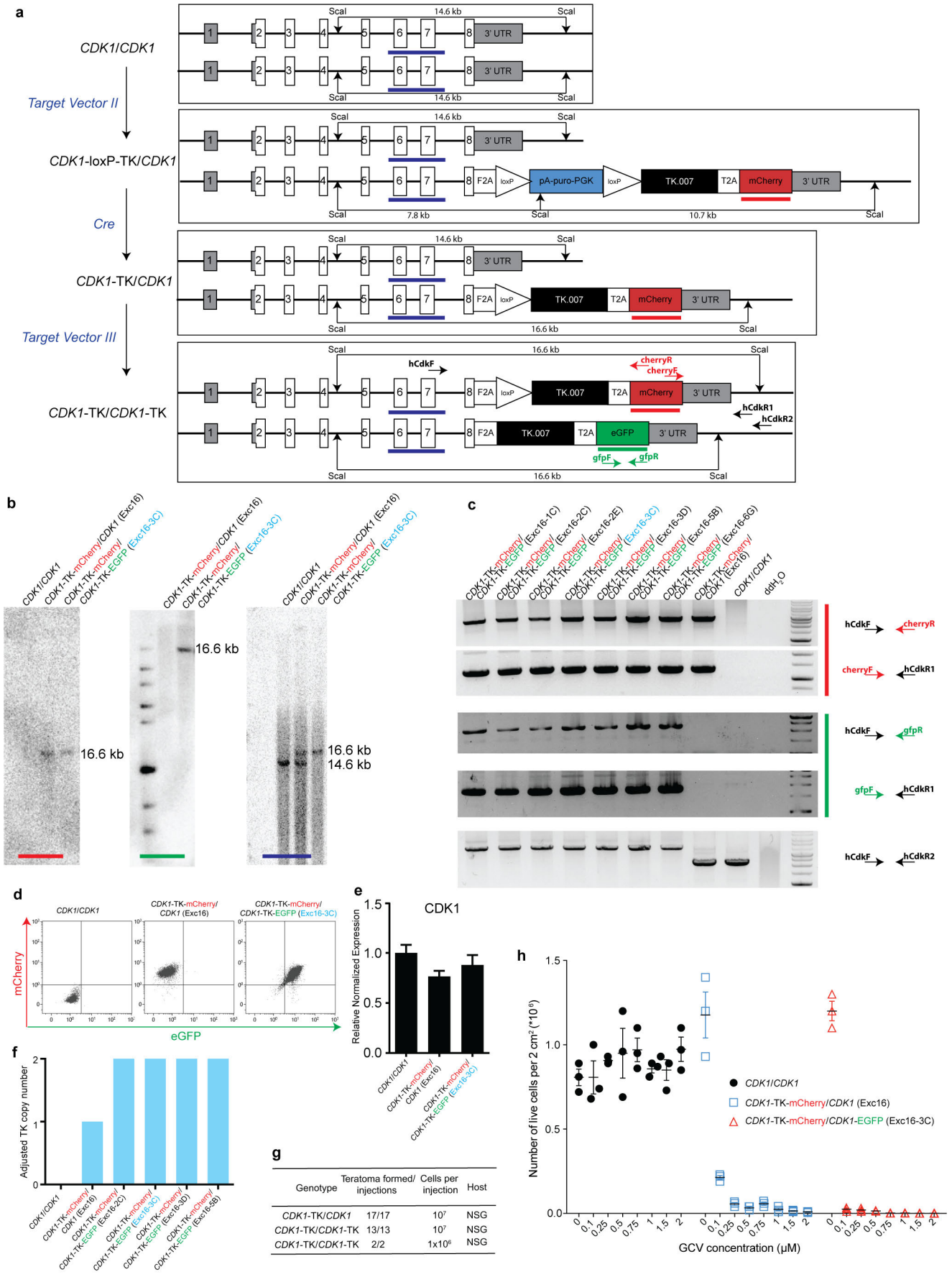

Genotype	Teratoma formed/ injections	Cells per injection	Host
CDK1-TK/*CDK1*	17/17	10^7	NSG
CDK1-TK/*CDK1*-TK	13/13	10^7	NSG
CDK1-TK/*CDK1*-TK	2/2	$1x10^6$	NSG

Extended Data Figure 3 | Generation, genotyping and characterization of human H1 *CDK1*-TK/*CDK1* and *CDK1*-TK/*CDK1*-TK ES cells. a, Steps of generating human H1 *CDK1*-TK/*CDK1* and *CDK1*-TK/*CDK1*-TK ES cells. **b**, Southern blot genotyping of the *CDK1*-TK/*CDK1* clone Exc16 used in teratoma assays (Fig. 1c and Extended Data Fig. 7) and the *CDK1*-TK/*CDK1*-TK clone Exc16-3C used in the differentiation assays in Fig. 3. **c**, PCR genotyping of all the correct clones. **d**, Flow cytometry analysis of the *CDK1*-TK/*CDK1* clone Exc16 and the *CDK1*-TK/*CDK1*-TK clone Exc16-3C. **e**, SybrGreen Q-PCR of human *CDK1* expression in H1 WT, the *CDK1*-TK/*CDK1* clone Exc16 and the *CDK1*-TK/*CDK1*-TK clone Exc16-3C. Values represent mean ± SD, n = 3. No significant difference among them. **f**, TaqMan Q-PCR copy number analysis of TKs of all the clones with the correct genotype. **g,** Table showing the efficiency of teratoma formation in NSG mice using H1 human ES cells. **h,** Dose-response analysis of wild type, *CDK1*-TK/*CDK1* and *CDK1*-TK/*CDK1*-TK human H1 ES cells. Cells were treated with different GCV concentrations, dissociated and counted after 7 days.

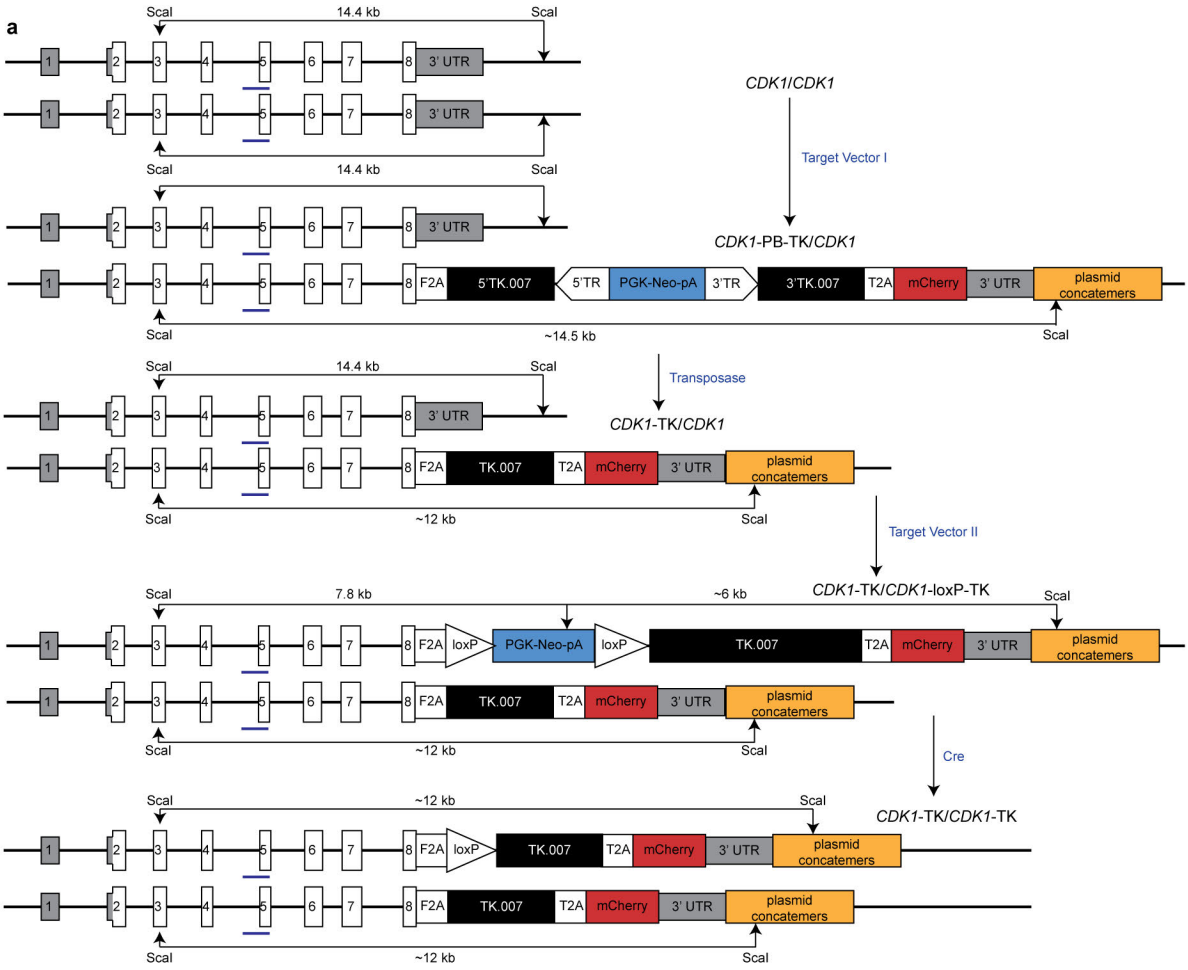

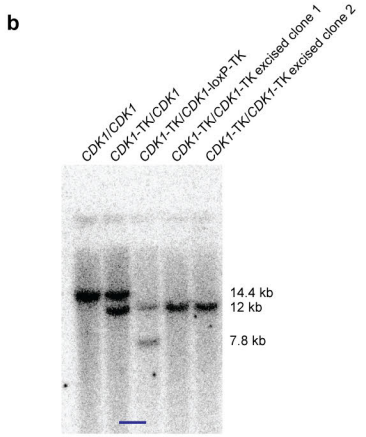

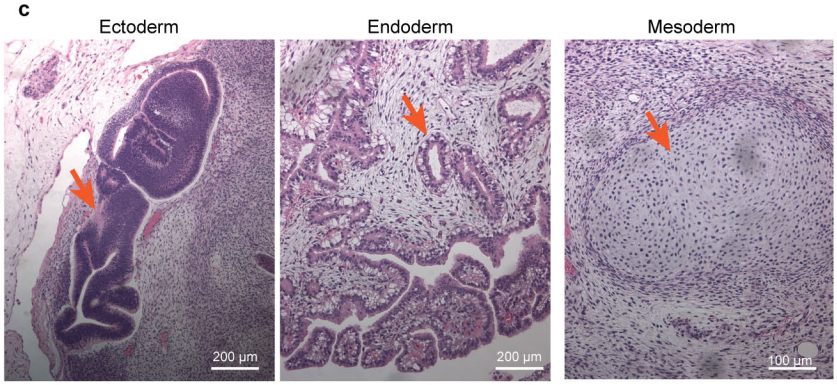

d

Genotype	Teratoma formed/ Injections	Cell number per injection	Host
CDK1-TK/*CDK1*-TK	4/4	1 - 4 x 10^6	NSG

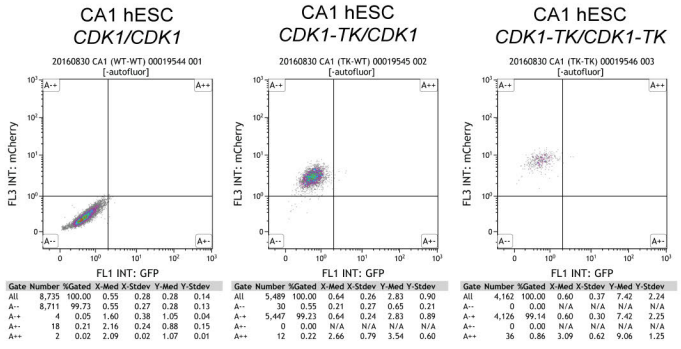

755

Extended Data Figure 4 | Generation, genotyping and characterization of human CA1 *CDK1*-TK/*CDK1* and *CDK1*-TK/*CDK1*-TK ES cells. a, Steps of generating human CA1 *CDK1*-TK/*CDK1* and *CDK1*-TK/*CDK1*-TK ES cells. **b**, Southern blot genotyping of human CA1 *CDK1*-TK/*CDK1* and *CDK1*-TK/*CDK1*-TK ES cells. The plasmid concatemers are multiple copies of plasmid integration (including backbone). The Ampicillin gene in the backbone contains a ScaI restriction enzyme site which is consistent with the sizes of the band in southern blots. **c**, H&E staining of a *CDK1*-TK/*CDK1*-TK CA1 ES cell derived teratoma.

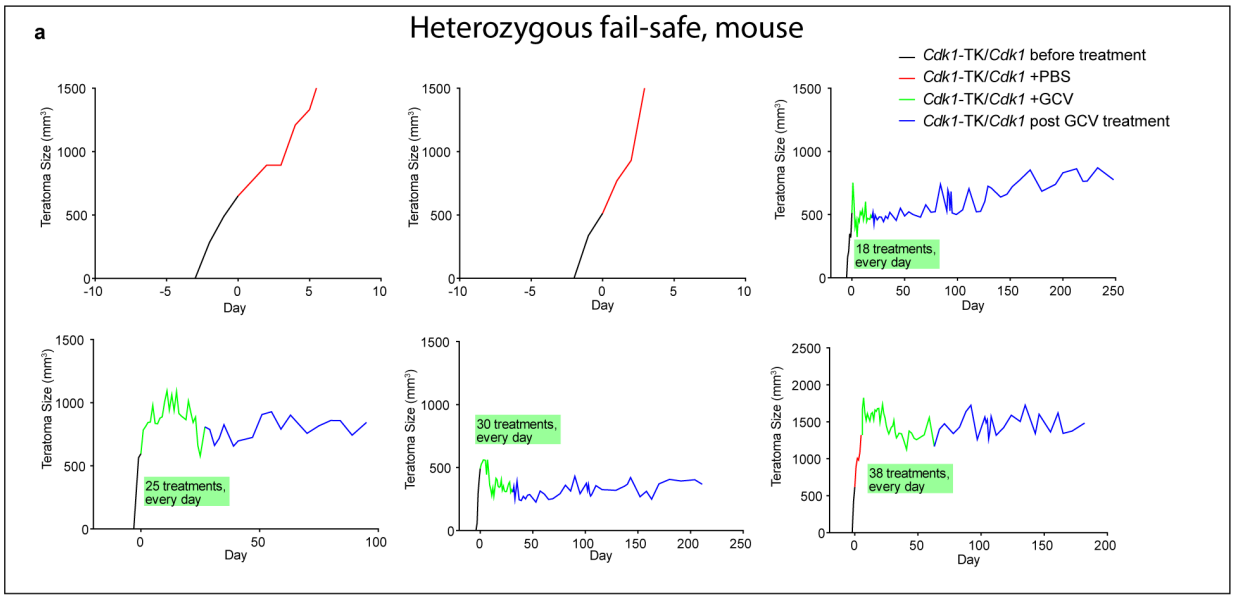
a
Heterozygous fail-safe, mouse
Cdk1-TK/Cdk1 before treatment
Cdk1-TK/Cdk1 +PBS
Cdk1-TK/Cdk1 +GCV
Cdk1-TK/Cdk1 post GCV treatment
Teratoma Size (mm³)
Day
18 treatments, every day
25 treatments, every day
30 treatments, every day
38 treatments, every day

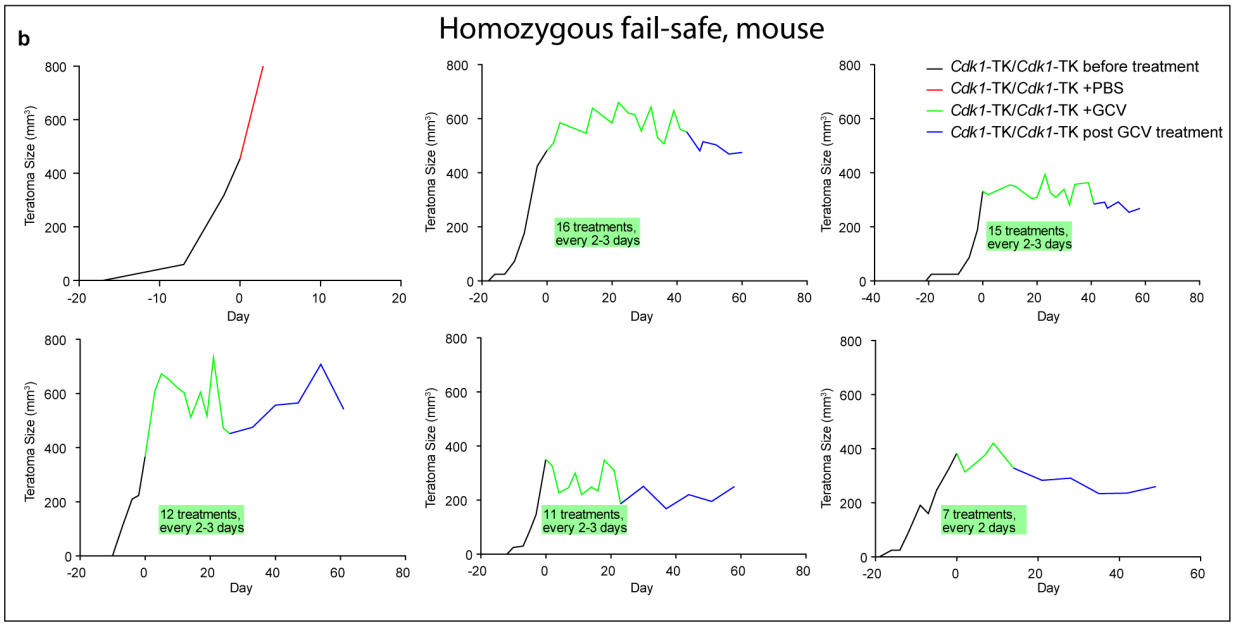
b
Homozygous fail-safe, mouse
Cdk1-TK/Cdk1-TK before treatment
Cdk1-TK/Cdk1-TK +PBS
Cdk1-TK/Cdk1-TK +GCV
Cdk1-TK/Cdk1-TK post GCV treatment
Teratoma Size (mm³)
Day
16 treatments, every 2-3 days
15 treatments, every 2-3 days
12 treatments, every 2-3 days
11 treatments, every 2-3 days
7 treatments, every 2 days

763

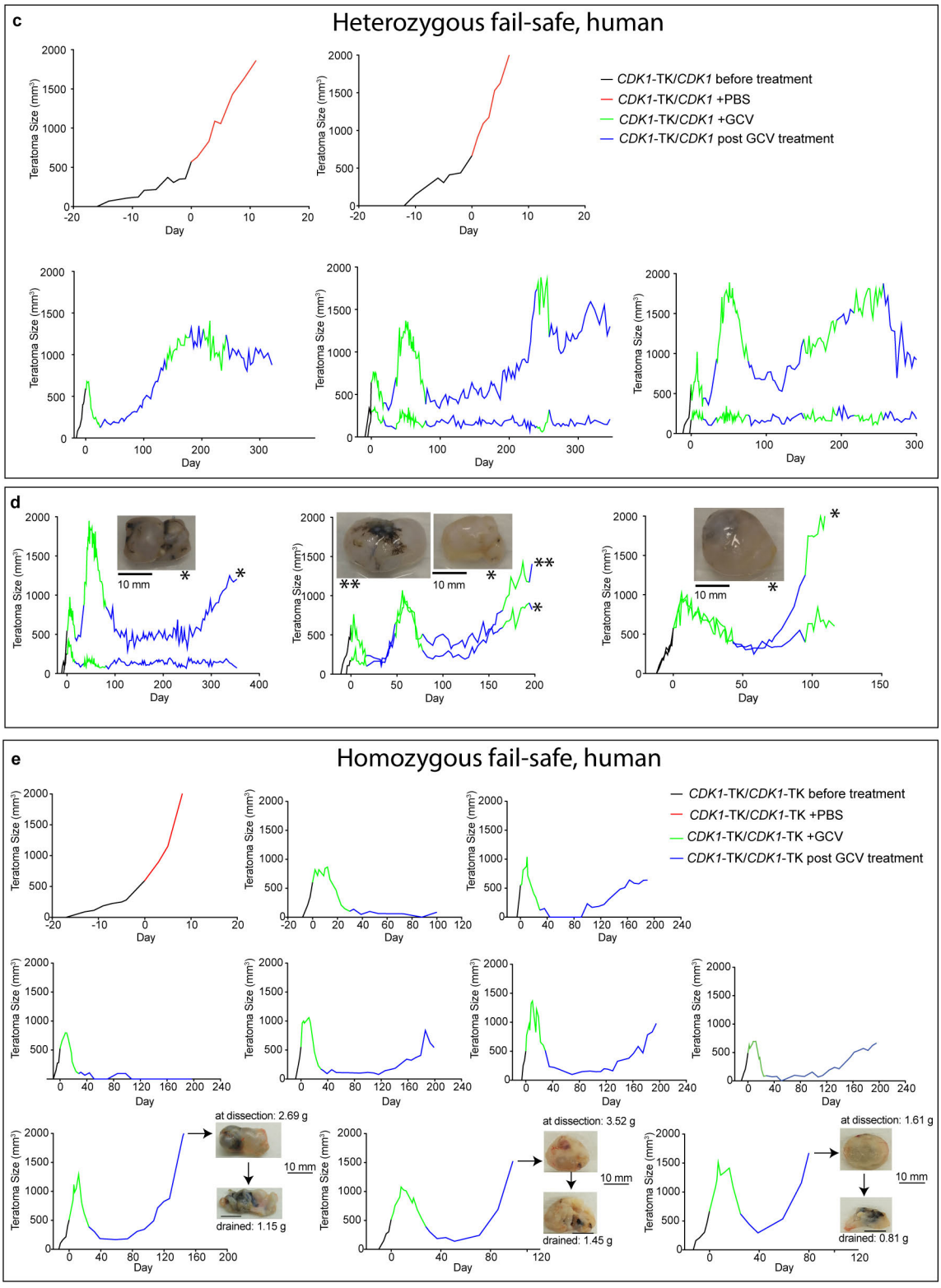

Extended Data Figure 5 | Growth graphs of mouse and human ES cells-derived teratomas. a, Growth of teratomas derived from mouse heterozygous fail-safe ES cells (C2 *Cdk1*-TK/*Cdk1)* **b**, Growth of teratomas derived from mouse homozygous fail-safe ES cells (C2 *Cdk1*-TK/*Cdk1*-TK) **c,** Growth of teratomas derived from human heterozygous fail-safe ES cells (H1 *CDK1*-TK/*CDK1*, clone Exc16), daily GCV treatment. **d,** Examples of teratomas from human heterozygous fail-safe ES cells

showing cyst formation, images of cystic teratomas at dissection are shown next to the corresponding growth line, daily GCV treatment. The graphs with two lines represent mice that had cells injected to both flanks. The graphs with one line represent mice that had cells injected to one flank. The GCV treatment regime varies among mice because each teratoma behaves differently; we started GCV when the teratoma size started to increase. **e,** Growth of teratomas derived from human homozygous fail-safe ES cells (H1 *CDK1*-TK/*CDK1*-TK), GCV treatment was every other day. Images of cystic teratomas are shown next to the corresponding growth line, cysts were drained after dissection to show the difference in tumour weight due to the fluid present in the tissue. Each graph represents one mouse.

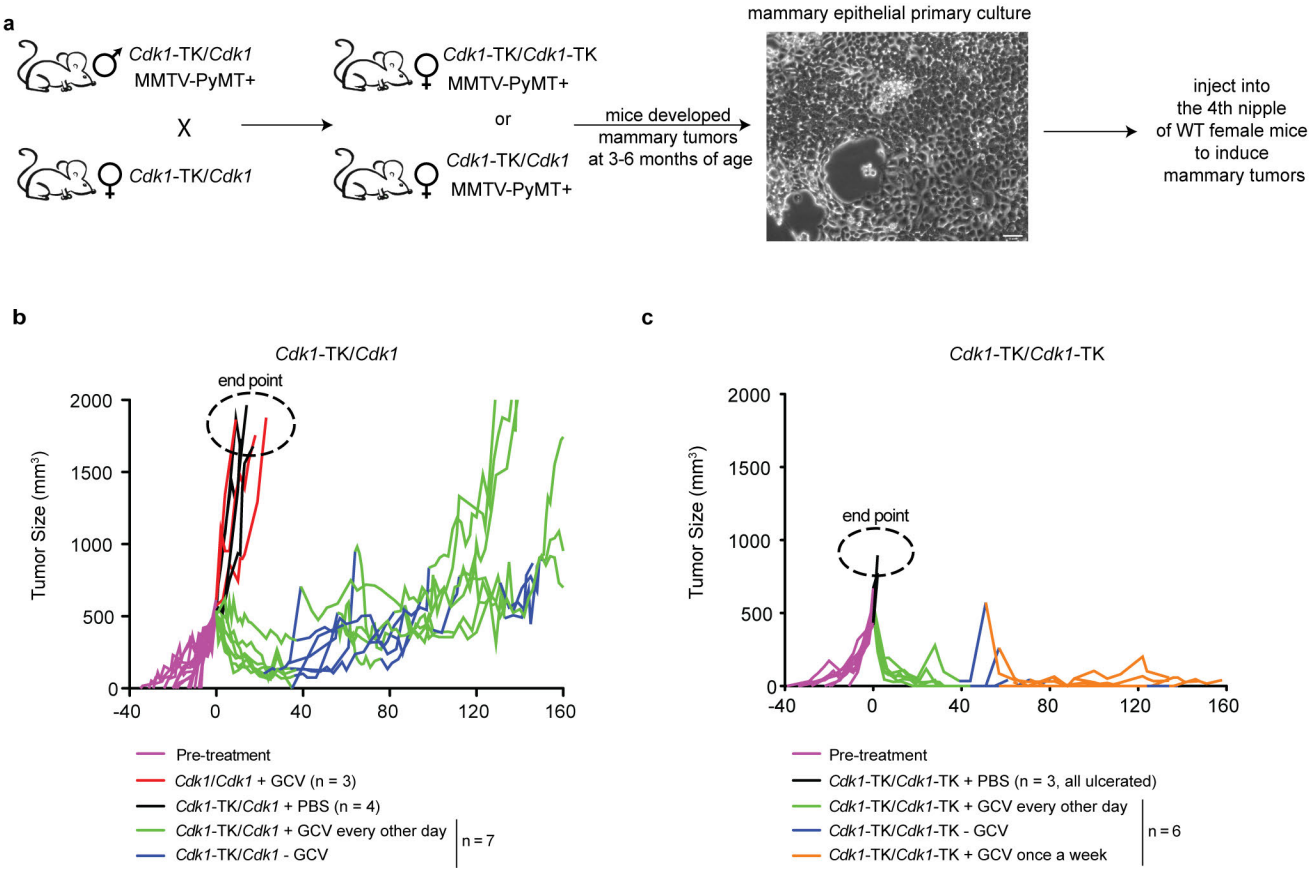

Extended Data Figure 6 | Breast cancer transplantation assay using heterozygous and homozygous FS mammary tumour cells. a, Generation of mouse line and experimental design. **b**, Growth of mammary gland tumours derived from mouse *Cdk1*/*Cdk1* and *Cdk1*-TK/*Cdk1* mammary epithelial cells with PBS or GCV treatment. **c,** Growth of mammary gland tumours derived from mouse *Cdk1*-TK/*Cdk1*-TK mammary epithelial cells with PBS or GCV treatment.

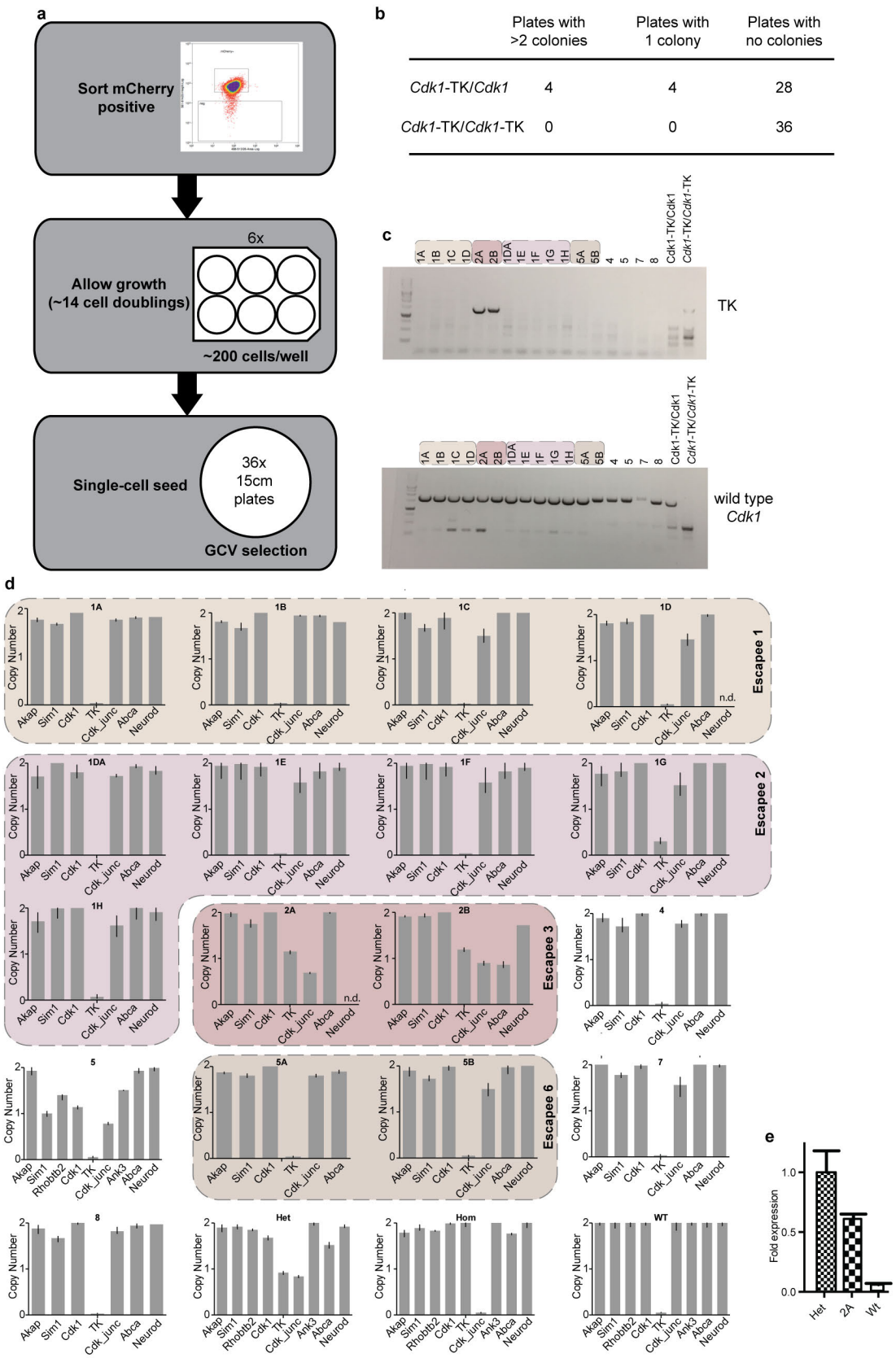

786
787
788 **Extended Data Figure 7 | *In vitro* experiments with mouse C2 *Cdk1*-TK/*Cdk1*, *Cdk1*-TK/*Cdk1*-TK ES**
789 **cells and subsequent characterization of escapees. a**, Experimental design: mCherry+ cells were

selected by sorting to ensure that the starting cell population did not contain escapees. These cells were plated on 6 well plates (200 cells/well, 36 total wells) and allowed to grow to 14 cell doublings (this was estimated by counting cells in sample wells). The 36 cultures were then resuspended to a single-cell suspension and each was plated to a 15 cm plate ($4x10^6$ cells). One day after plating, selection with GCV was started and maintained until escapee colonies appeared. **b**, Escapee numbers obtained in 36 independent cultures growing from *Cdk1*-TK/*Cdk1*, *Cdk1*-TK/*Cdk1*-TK ES cells. **c**, PCR to determine the presence of TK. **d**, TaqMan copy number Q-PCR analysis of *Akap*, *Sim1*, *Cdk1* junction of exon 8 and 3'UTR, *Neurod*, *Cdk1*, *TK*, *Abca* on mouse Chr. 10. Values represent the copy number calculated by CopyCaller Software v2.1 and the bars indicate the range from the minimum to the maximum number. n = 3. The same color in the background of **c** and **d** indicates that they are from the same independent culture. **e**, Q-PCR to compare TK expression level in *Cdk1*-TK/*Cdk1* escapee clone 2A and C2 WT ES cells. Values represent mean ± SEM. n = 3.

a

Number of replicate culture	Initial number of cells per culture	Average number of cells/ culture	Total numbers of cells	Total live cells analyzed	Live cells / total cells	Average mutants per sample	LOH rate per cell division
21	1	$4.9x10^6$	$4.9x10^6x21=1.029x10^8$	18,833,305	0.18	eGFP only: 303	mCherry loss frequency: $9.05x10^{-6}$
						mCherry only: 251	eGFP loss frequency: $7.68x10^{-6}$

b

Samples	All events	Live cells	Single cells	eGFP+ mCherry-	mCherry+ eGFP-
1	50,000	36,102	14,261	0	1
2	1,387,922	1,166,927	663,704	11	32
3	1,306,685	1,229,940	734,030	59	95
4	1,977,744	1,473,607	1,229,131	29	38
5	2,492,764	2,051,819	1,798,915	114	114
6	2,639,618	2,160,508	1,891,409	102	108
7	559,819	406,149	374,528	18	3
8	39,161	15,380	12,977	0	1
9	1,661,726	1,354,148	1,153,558	156	81
10	2,315,402	1,911,681	1,664,292	63	75
11	843,549	611,761	529,324	124	45
12	2,088,898	1,595,412	1,337,789	86	69
13	2,468,994	1,853,728	1,628,365	69	75
14	92,019	56,795	46,791	10	9
15	1,791,662	1,076,661	953,464	7	4
16	2,153,934	1,680,018	1,485,732	179	106
17	1,416,523	1,029,636	882,532	7	8
18	1,096,211	771,314	653,076	32	25
19	15,695	8,297	6,665	1	0
20	764,311	598,206	533,928	28	6
21	1,802,185	1,369,832	1,238,834	72	73
Total	**28,964,822**	**22,457,921**	**18,833,305**	**1,167**	**968**
Total mutants in all samples				6,376.16	5,288.89
Average mutants per sample				303.62	251.85
Mutation rate				$9.05x10^{-6}$	$7.68x10^{-6}$

Extended Data Figure 8 | Calculation of the LOH rate at the human *CDK1* locus with human H1 *CDK1*-TK/*CDK1*-TK ES cells. a, Summary table. **b**, Detailed cell number for each individual clone.

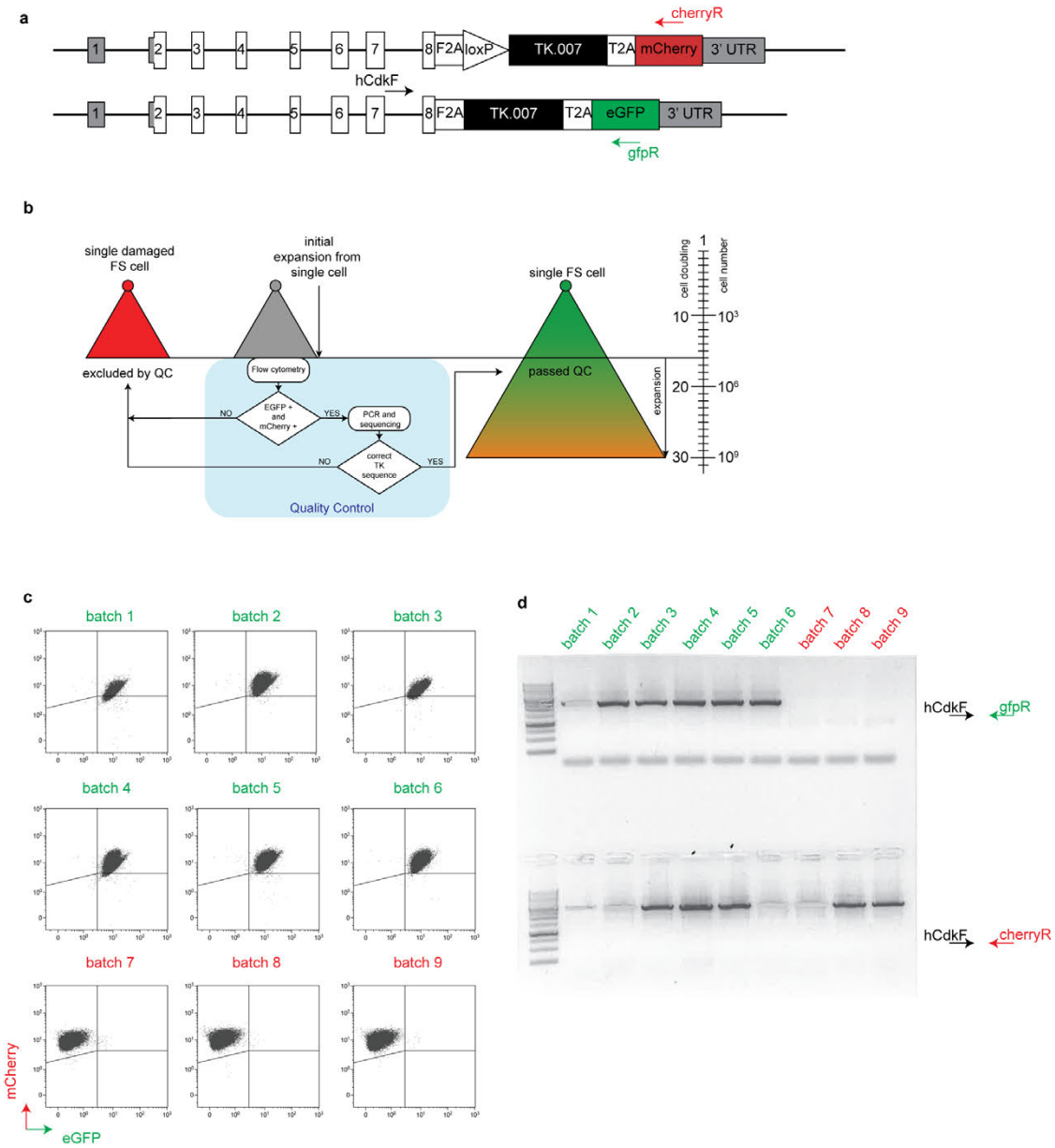

Extended Data Figure 9 | Quality control (QC) of batches generated from single human H1 *CDK1*-TK/*CDK1*-TK ES cells. a, Schematics of the alleles in the *CDK1*-TK/*CDK1*-TK human ES cells used in the quality control. **b**, Workflow schematic of performing QC on several ES cell batches. **c**, An example of the flow cytometry for the QC of nine clonally derived batches. **d**, An example of PCR for the QC of nine clonally derived batches.

812

a

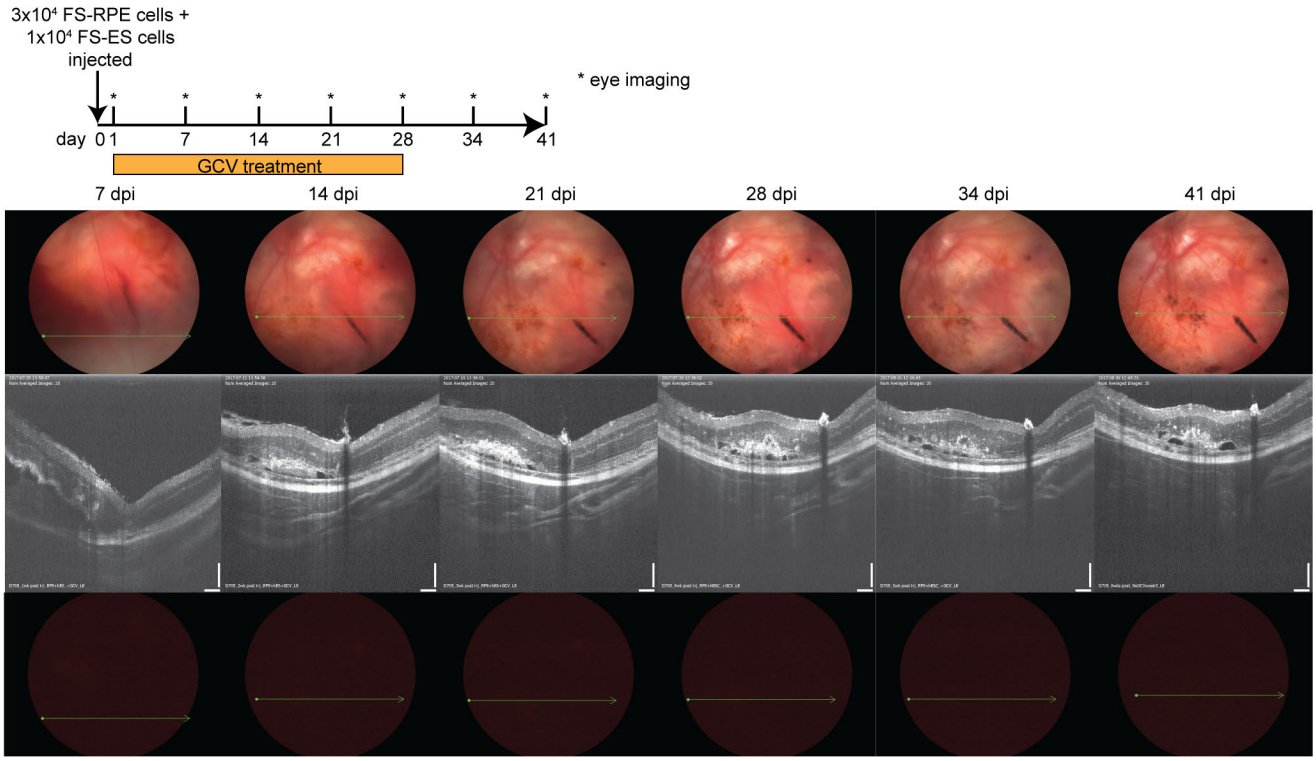
3x10⁴ FS-RPE cells +
1x10⁴ FS-ES cells
injected
* eye imaging
day 0 1 7 14 21 28 34 41
GCV treatment
7 dpi
14 dpi
21 dpi
28 dpi
34 dpi
41 dpi

b

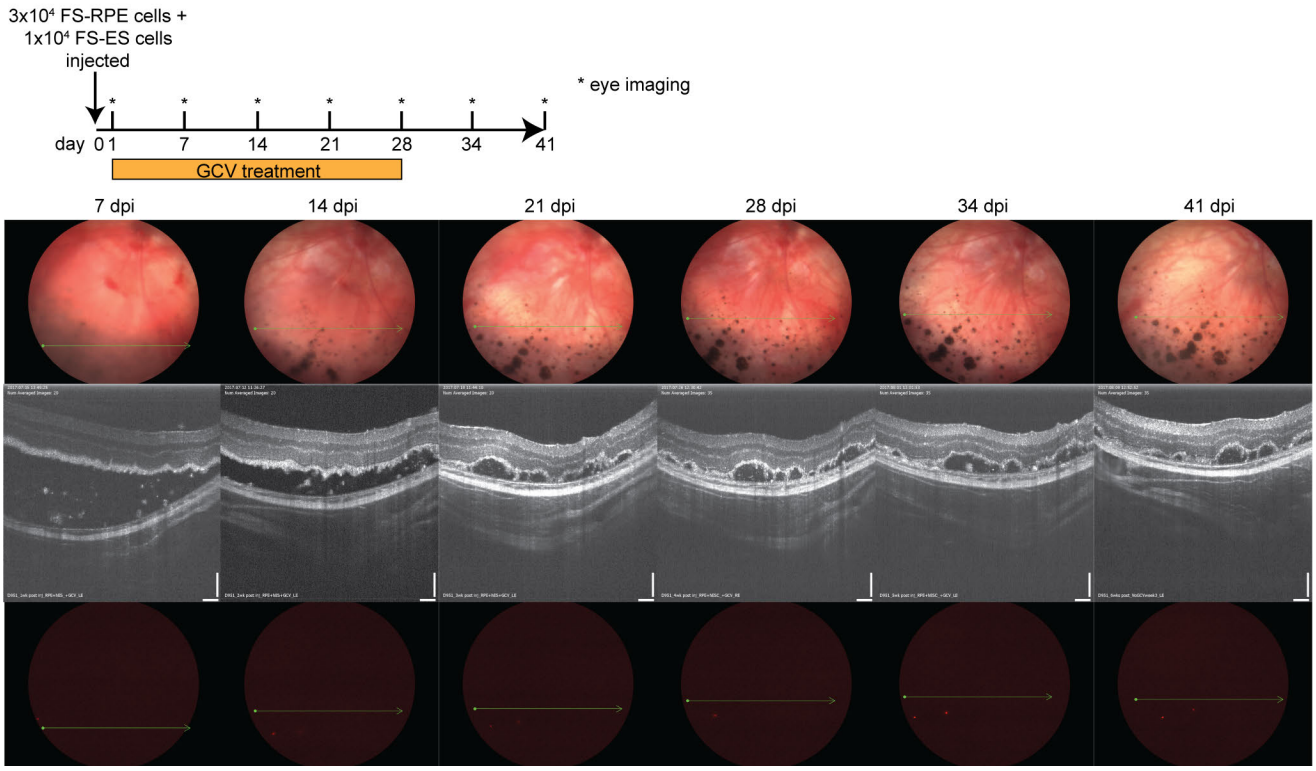
3x10⁴ FS-RPE cells +
1x10⁴ FS-ES cells
injected
* eye imaging
day 0 1 7 14 21 28 34 41
GCV treatment
7 dpi
14 dpi
21 dpi
28 dpi
34 dpi
41 dpi

813

c

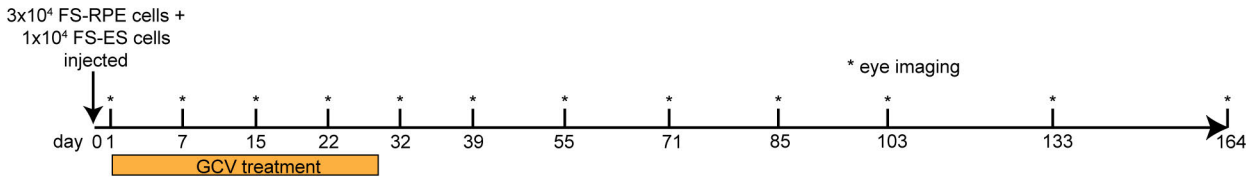
3x10⁴ FS-RPE cells +
1x10⁴ FS-ES cells
injected
* eye imaging
day 0 1 7 15 22 32 39 55 71 85 103 133 164
GCV treatment

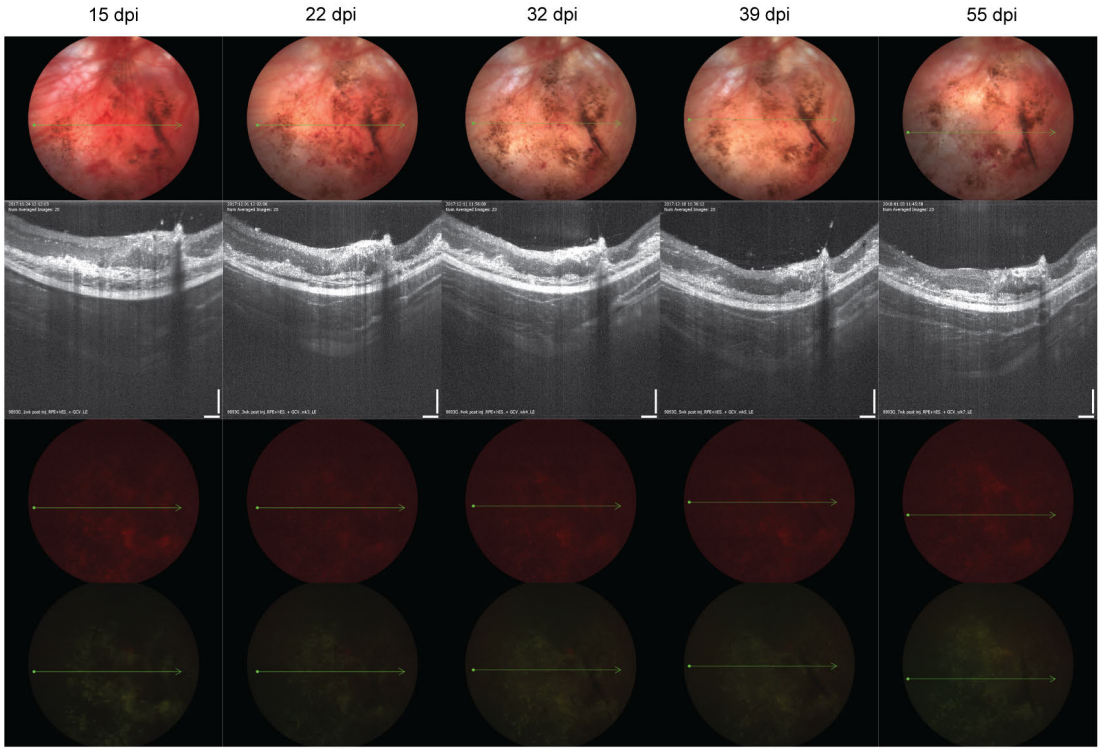
15 dpi
22 dpi
32 dpi
39 dpi
55 dpi

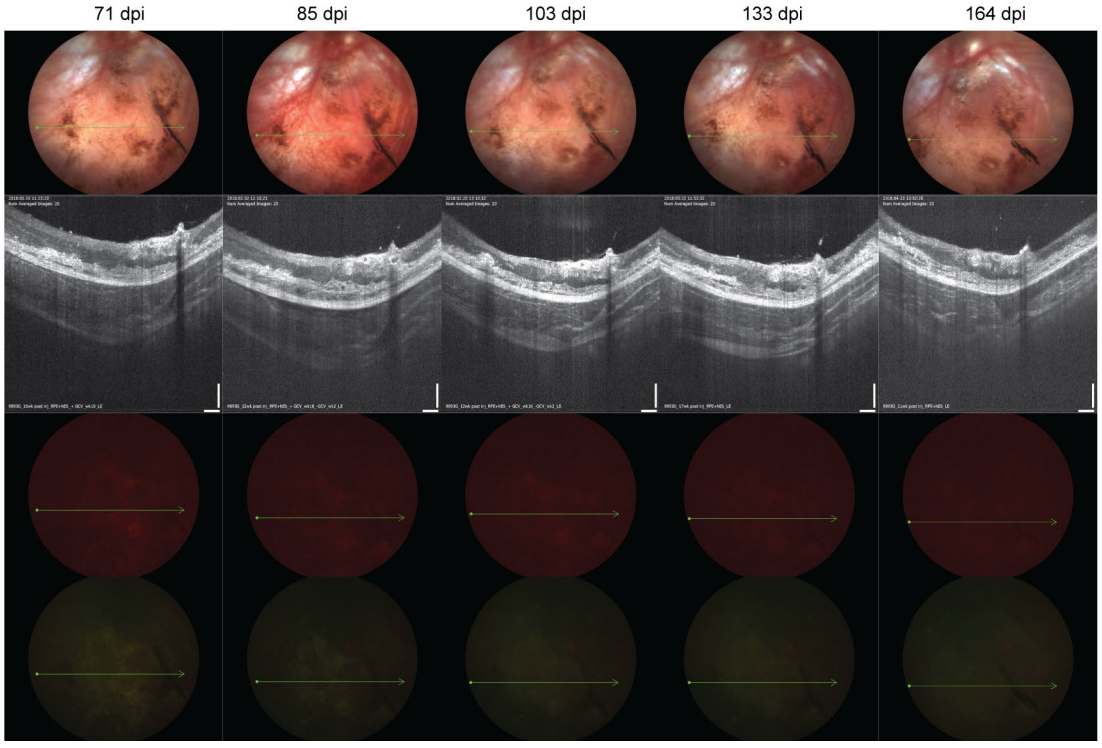
71 dpi
85 dpi
103 dpi
133 dpi
164 dpi

814

d

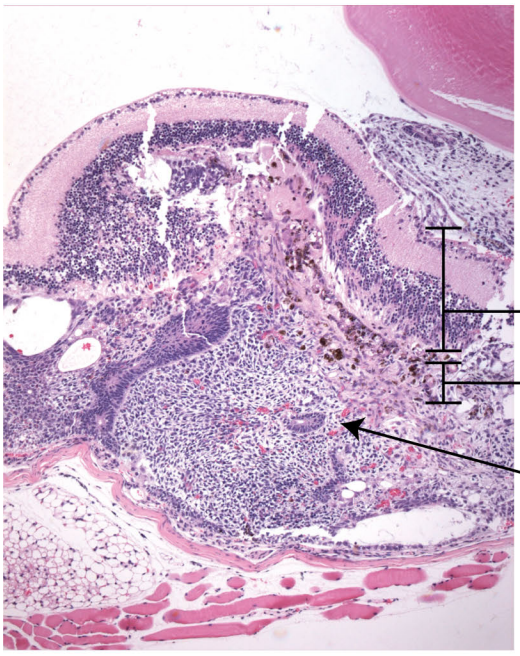
host retina
injected RPE
ES derived teratoma

e

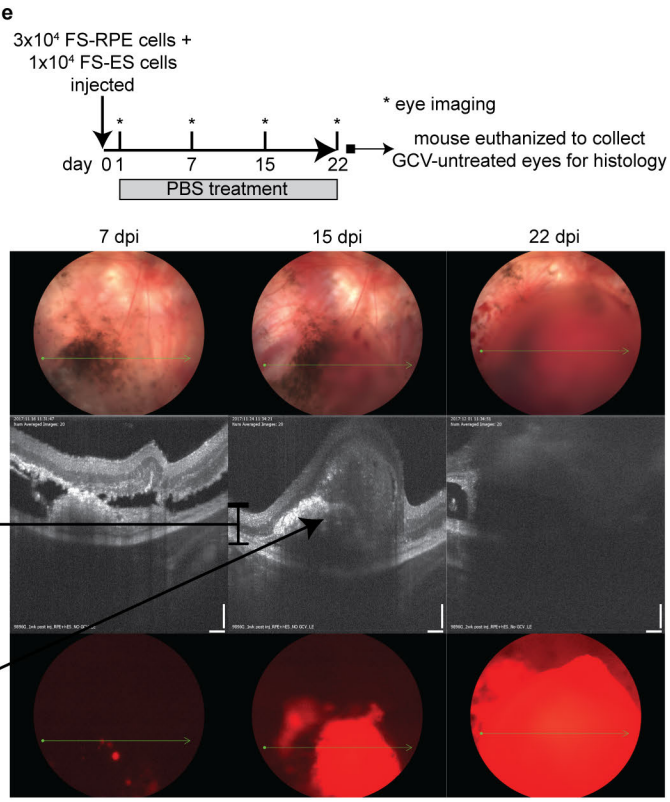
3x10⁴ FS-RPE cells + 1x10⁴ FS-ES cells injected
* eye imaging
mouse euthanized to collect GCV-untreated eyes for histology
day 0 1 7 15 22
PBS treatment
7 dpi
15 dpi
22 dpi

f

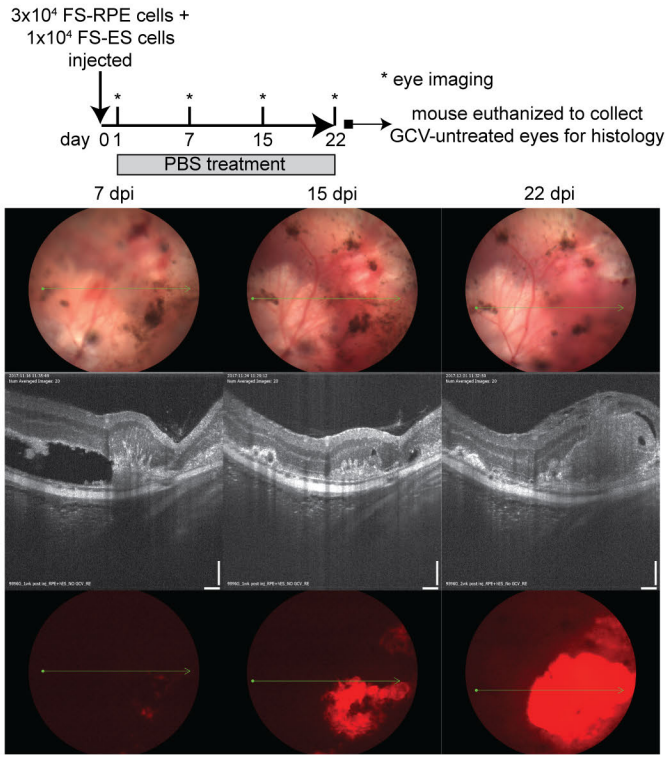
3x10⁴ FS-RPE cells + 1x10⁴ FS-ES cells injected
* eye imaging
mouse euthanized to collect GCV-untreated eyes for histology
day 0 1 7 15 22
PBS treatment
7 dpi
15 dpi
22 dpi

g

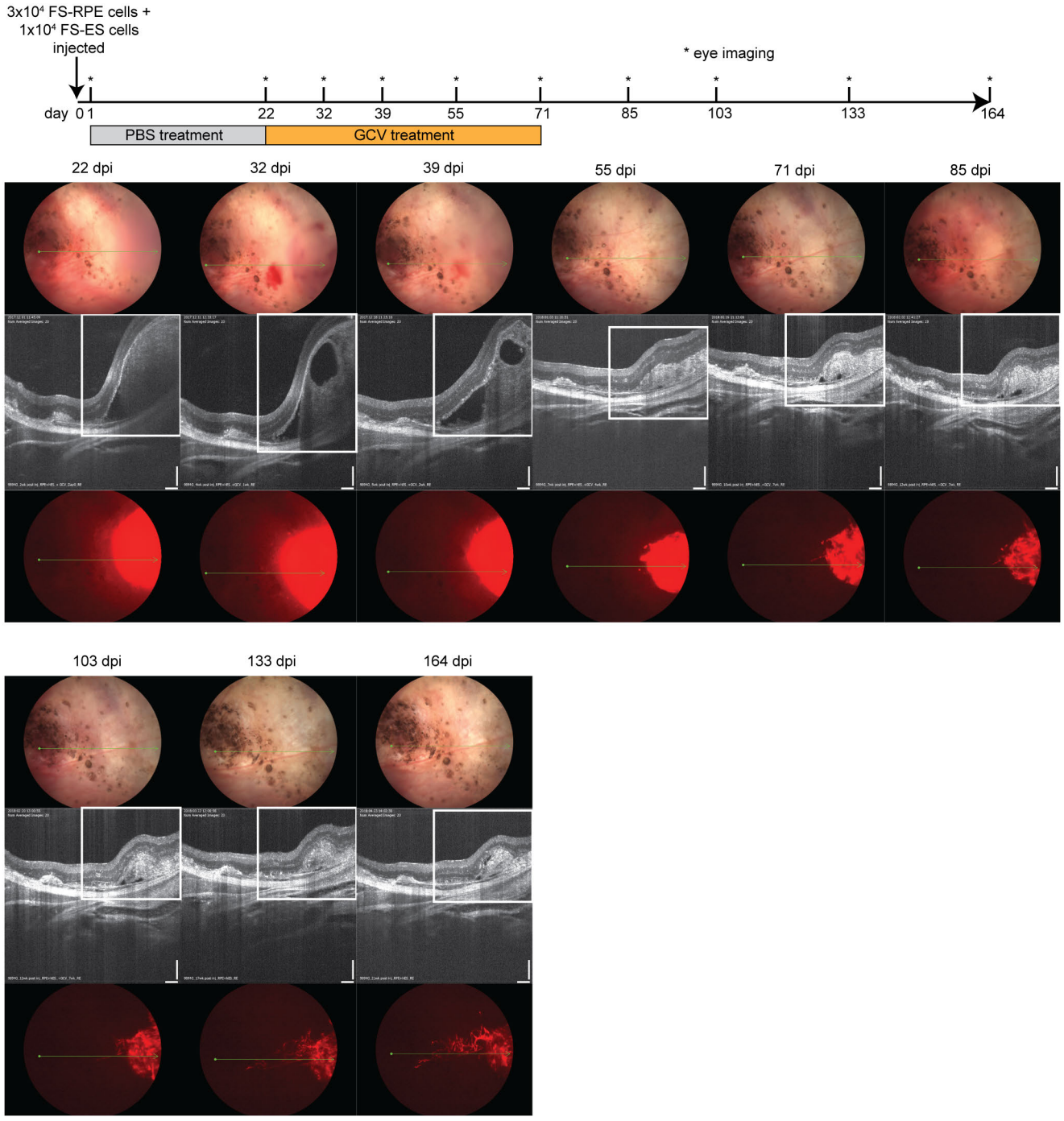
3x10⁴ FS-RPE cells +
1x10⁴ FS-ES cells
injected
* eye imaging
day 0 1 22 32 39 55 71 85 103 133 164
PBS treatment
GCV treatment
22 dpi
32 dpi
39 dpi
55 dpi
71 dpi
85 dpi
103 dpi
133 dpi
164 dpi

816

h

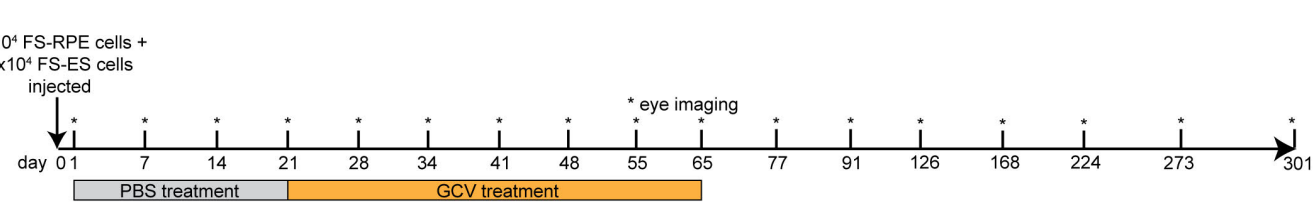
3x10⁴ FS-RPE cells +
1x10⁴ FS-ES cells
injected
* eye imaging
day 0 1 7 14 21 28 34 41 48 55 65 77 91 126 168 224 273 301
PBS treatment
GCV treatment

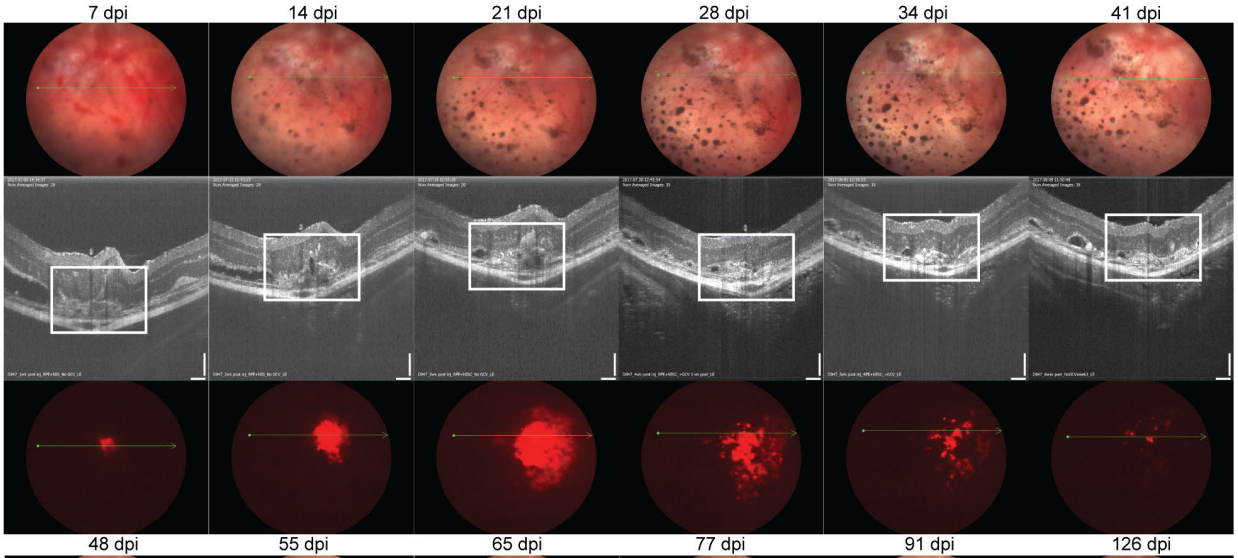
7 dpi
14 dpi
21 dpi
28 dpi
34 dpi
41 dpi

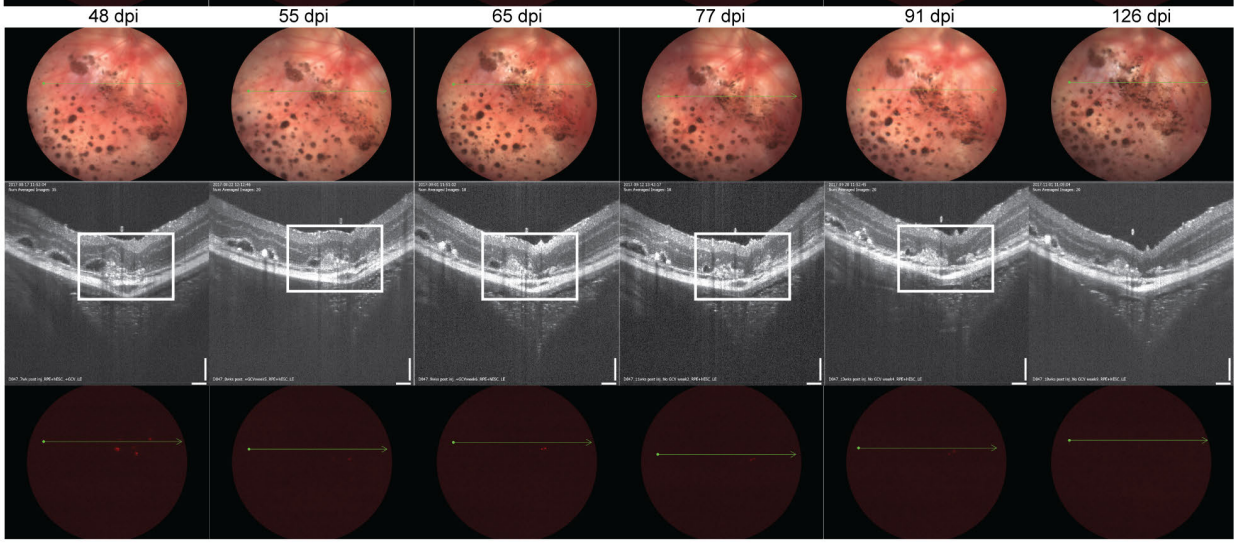
48 dpi
55 dpi
65 dpi
77 dpi
91 dpi
126 dpi

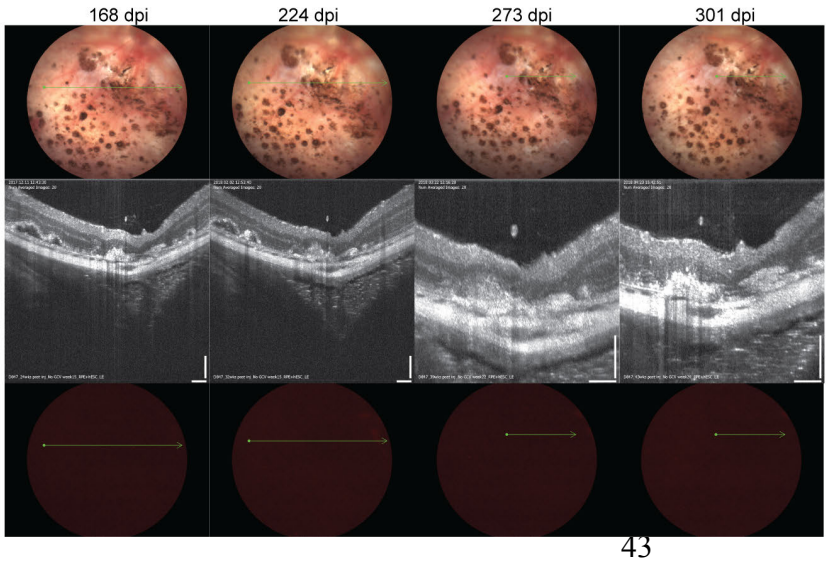
168 dpi
224 dpi
273 dpi
301 dpi

817

818

i

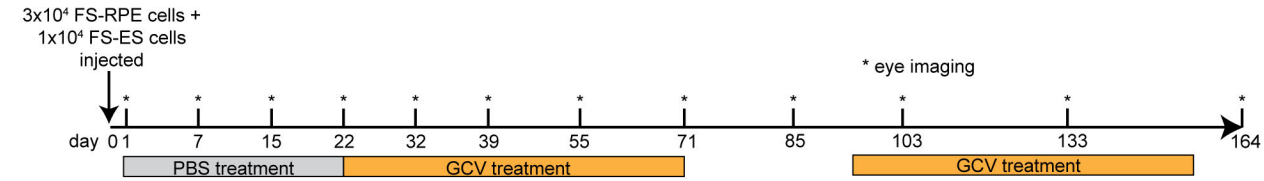
3x10⁴ FS-RPE cells +
1x10⁴ FS-ES cells
injected
* eye imaging
day 0 1 7 15 22 32 39 55 71 85 103 133 164
PBS treatment
GCV treatment
GCV treatment

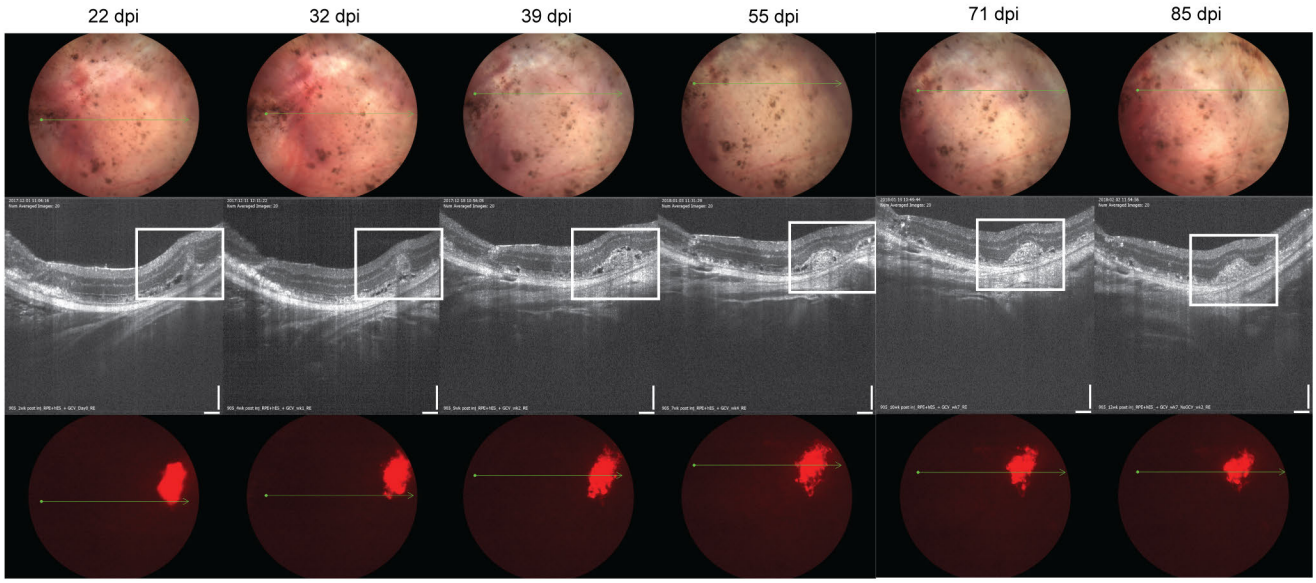
22 dpi
32 dpi
39 dpi
55 dpi
71 dpi
85 dpi

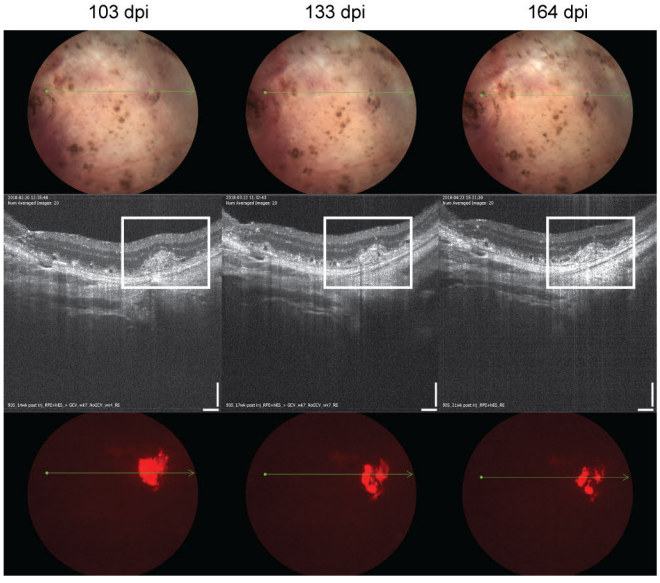
103 dpi
133 dpi
164 dpi

819

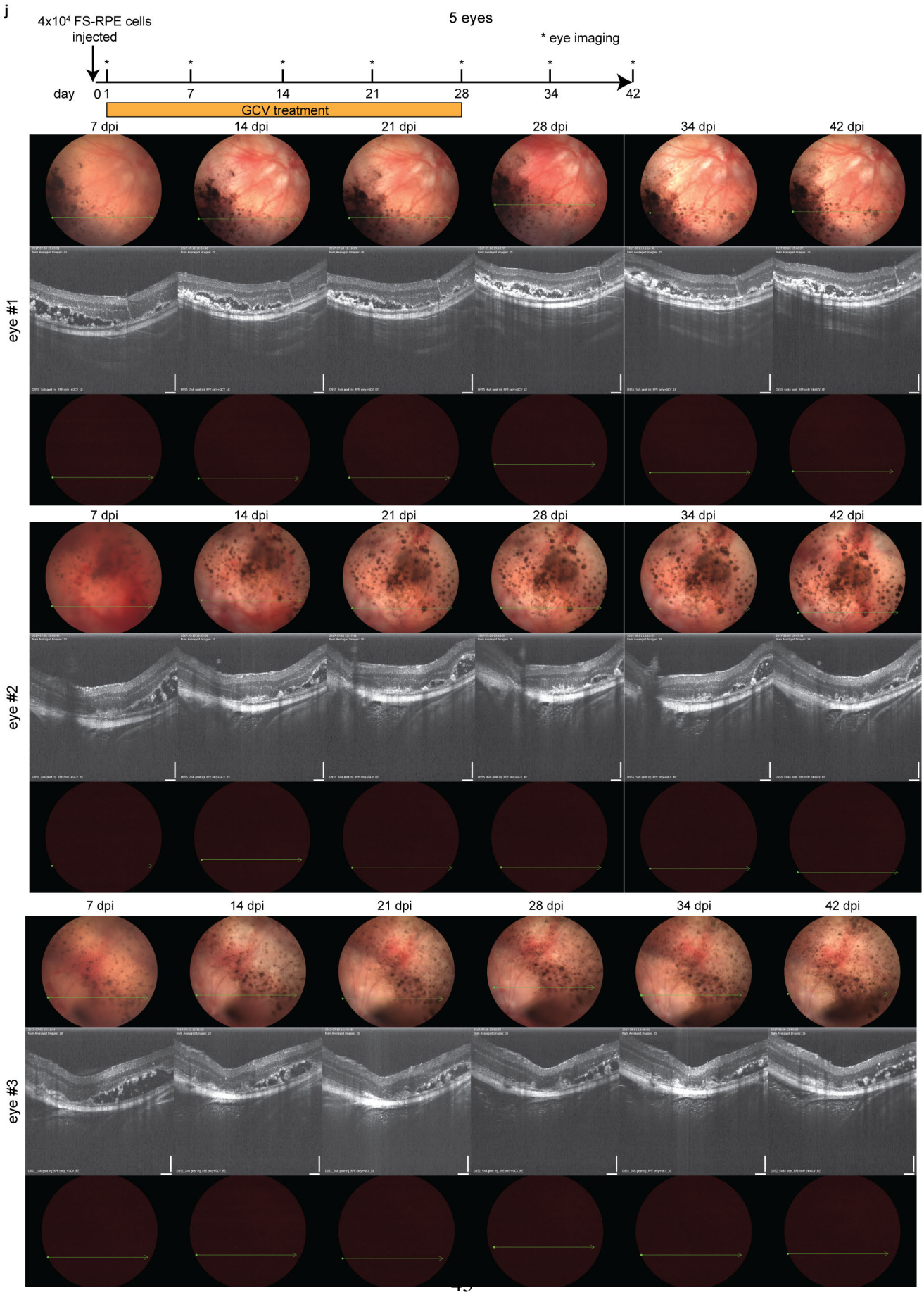
j
4x10⁴ FS-RPE cells injected
5 eyes
* eye imaging
day 0 1 7 14 21 28 34 42
GCV treatment
7 dpi
14 dpi
21 dpi
28 dpi
34 dpi
42 dpi
eye #1
eye #2
eye #3

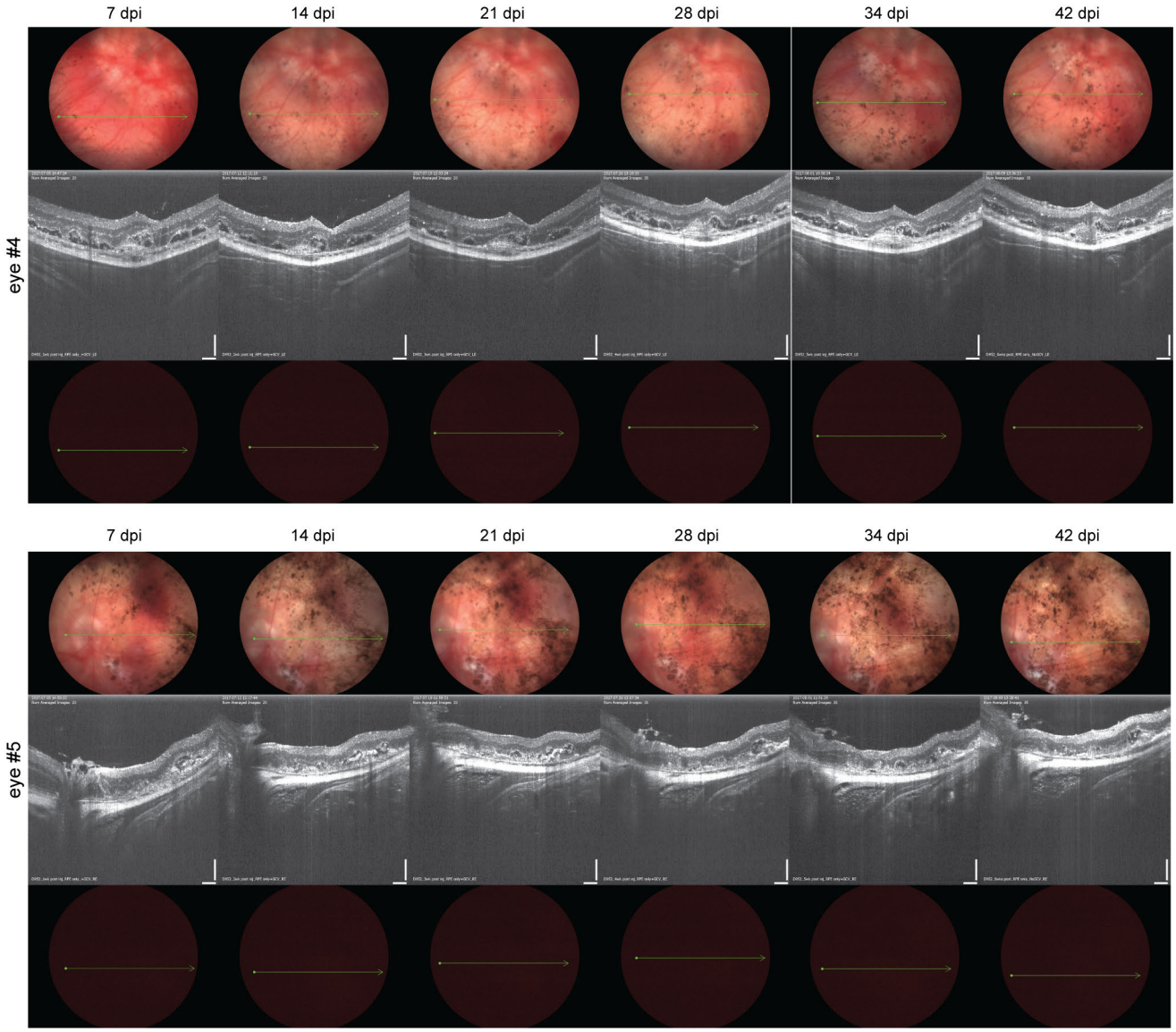
7 dpi
14 dpi
21 dpi
28 dpi
34 dpi
42 dpi
eye #4
7 dpi
14 dpi
21 dpi
28 dpi
34 dpi
42 dpi
eye #5

821

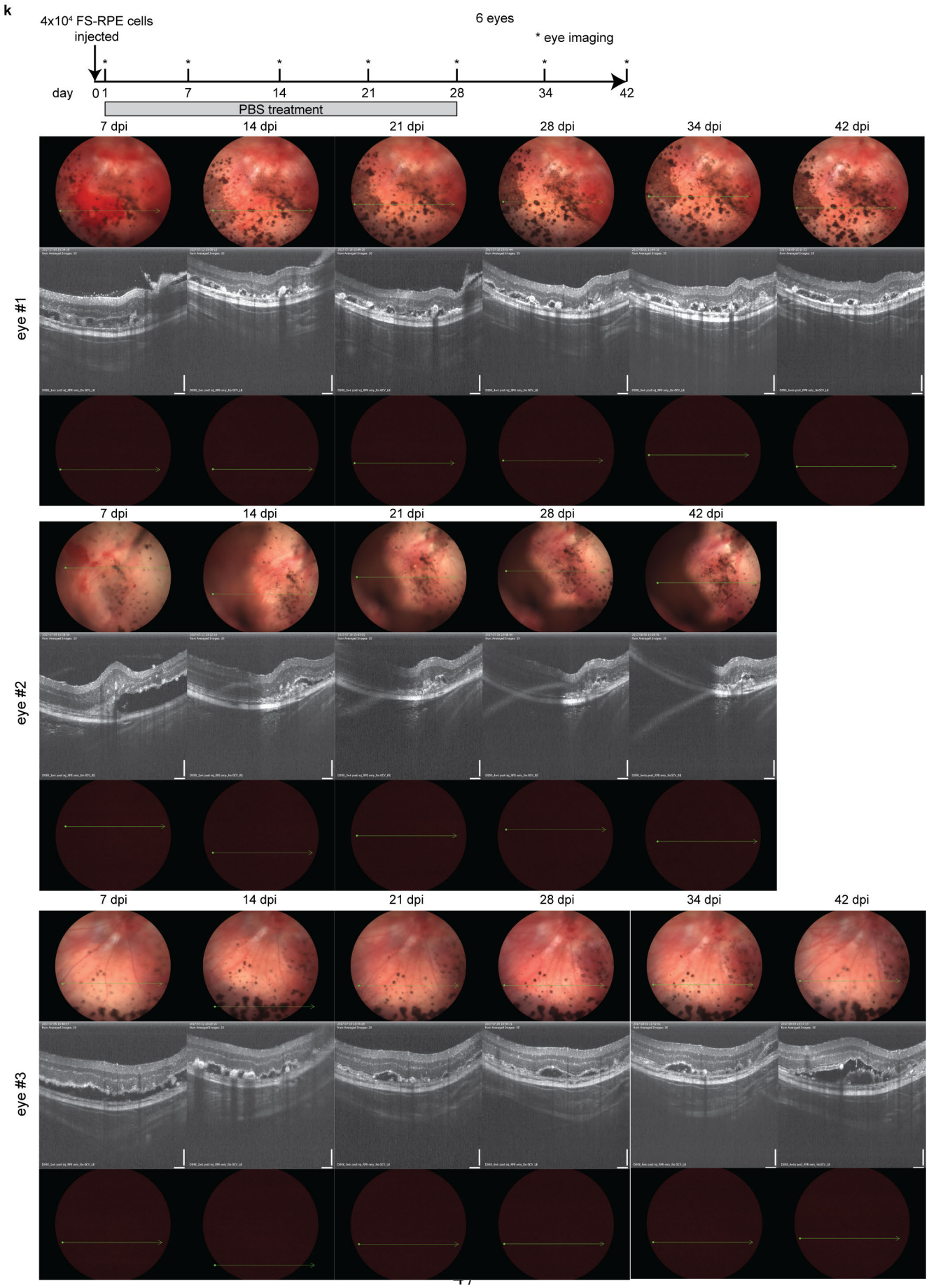
k
4x10⁴ FS-RPE cells injected
6 eyes
* eye imaging
day 0 1 7 14 21 28 34 42
PBS treatment
7 dpi
14 dpi
21 dpi
28 dpi
34 dpi
42 dpi
eye #1
eye #2
eye #3

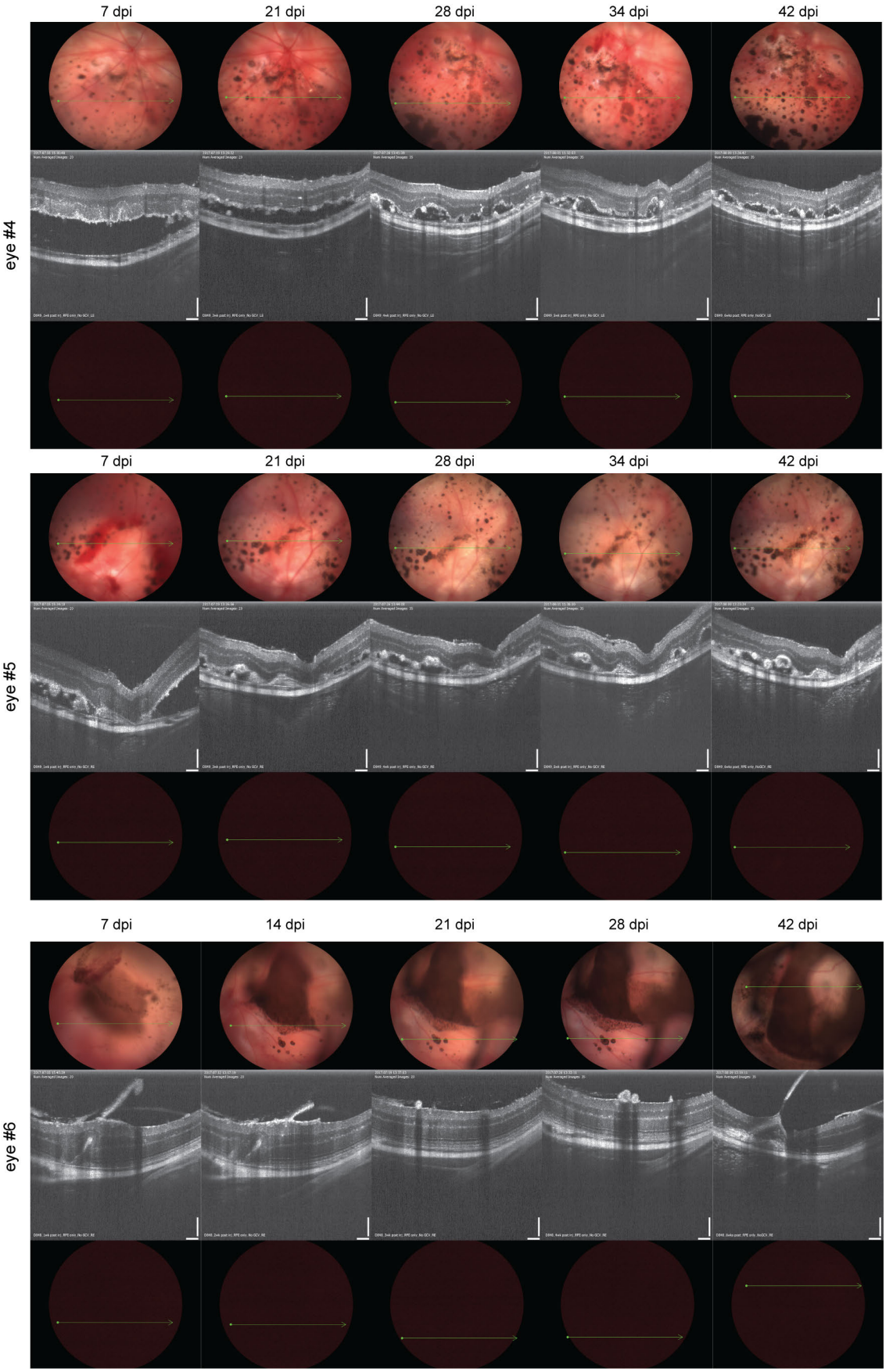
7 dpi
21 dpi
28 dpi
34 dpi
42 dpi
eye #4
7 dpi
21 dpi
28 dpi
34 dpi
42 dpi
eye #5
7 dpi
14 dpi
21 dpi
28 dpi
42 dpi
eye #6

823

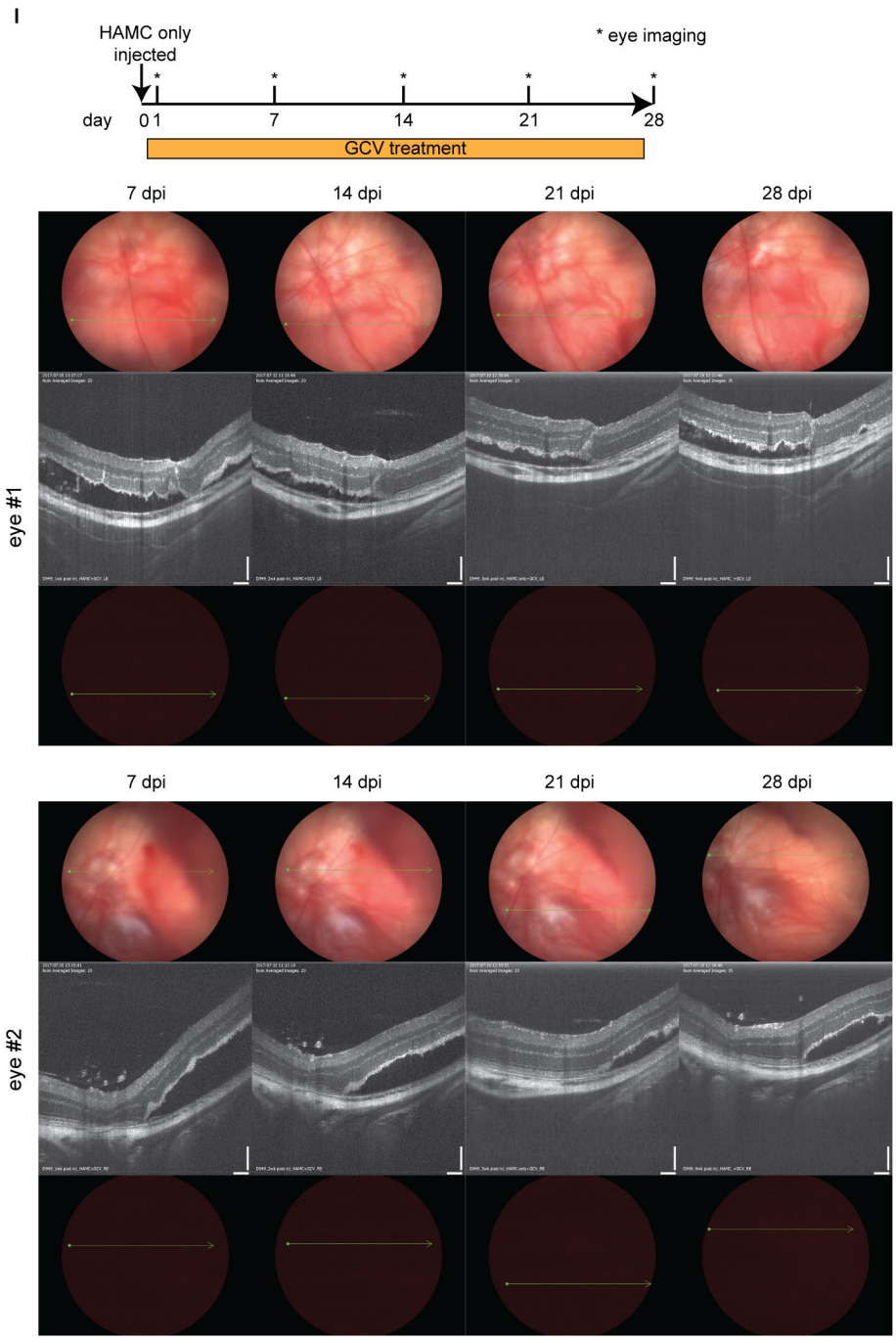

Extended Data Figure 10 | Images of all eyes co-transplanted with FS-RPE and FS-ES cells (in addition to Fig. 4), and images of all the eyes transplanted only with FS-RPE cells. a-c, Fundoscopy, OCT and fluorescence imaging of eyes co-transplanted with FS-RPE and FS-ES cells (4-week GCV treatment). The absence of mCherry signal indicates that ES cell growth has not occurred. The bottom panel in **c** includes the green fluorescence channel to illustrate that the observed signal in the red fluorescence channel is actually autofluorescence. **d,** Histological analysis of the eye presented in **e**. **e-i**, Fundoscopy, OCT and fluorescence imaging of eyes co-transplanted with FS-RPE and FS-ES cells (PBS treatment). mCherry signal is detectable and indicates ES cell growth. GCV treatment began 3 weeks post-injection following an initial PBS treatment. **j**, Fundoscopy, OCT and fluorescence imaging of eyes receiving only FS-RPE cells (4-week GCV treatment). This demonstrates that GCV treatment did not affect the RPE cells. **k**, Fundoscopy, OCT and fluorescence imaging of eyes receiving only FS-

RPE cells (4-week PBS treatment). **l**, Fundoscopy, OCT and fluorescence imaging of eyes receiving only HAMC (4-week GCV treatment).

Supplementary Calculation 1
The Effect of Aliquoting on FSL Calculation

We consider a pool of $N = 2^n$ cells that has $FSL_p = 1/p$ for some $p \in (0, 1)$. This means p is the probability that the pool of cells is not FS. Below we calculate first the probability that a randomly selected cell aliquot of size $M = 2^m$, $m < n$ is FS, i.e., the probability that it contains only FS cells.

In our model the pool can have 2^k non-FS cells with probability p_k, for $k = 0, 1, ..., n$, such that $p_{k+1} = p_k/2$ for $k = 0, 1, 2, 3, ..., n-1$. Thus

$$p_k = p_{k-1}/2 = p_{k-2}/2^2 = ... = p_0/2^k,$$

for $k = 1, 2, ..., n$, and since $1 - p$ is the probability that the pool is FS, we have

$$1 = 1 - p + \sum_{j=0}^{n} p_k = 1 - p + p_0(1 + 2^{-1} + ... + 2^{-n}) = 1 - p + p_0(2 - 2^{-n}).$$

Hence

$$p_0 = \frac{p}{2 - 2^{-n}}, \quad p_k = p2^{-k}(2 - 2^{-n})^{-1}, \quad k = 0, 1, ..., n.$$

Let q_a denote the probability that the aliquot is FS, and let $q_{a|k}$ denote the conditional probability that the aliquot is FS given that the pool has 2^k non-FS cells. Clearly, the conditional probability that the aliquot is FS, given that the pool is FS, is 1, and $q_{a|k} = 0$ if $N - 2^k < M$, i.e., when $k \geq n$. Thus by the law of total probability

$$q_a = 1 - p + \sum_{k=0}^{n} p_k q_{a|k} = 1 - p + p \sum_{k=0}^{n-1} 2^{-k}(2 - 2^{-n})^{-1} q_{a|k}. \tag{1}$$

It remains to calculate $q_{a|k}$. To this end we imagine that we choose M cells randomly, consecutively and without replacement, from a pool of size N which has $K := 2^k$ non-FS cells. The probabilities that the first chosen cell is FS, the second chosen cell is FS and that the j-th chosen cell is FS, are $\frac{N-K}{N}$, $\frac{N-K-1}{N-1}$ and $\frac{N-K-j+1}{N-j+1}$, respectively, for $j < N - K$. Hence

$$q_{a|k} = \tfrac{N-K}{N} \times \tfrac{N-K-1}{N-1} \times \cdots \times \tfrac{N-K-M+1}{N-M+1} = \Pi_{j=0}^{M-1} \tfrac{N-K-j}{N-j}. \tag{2}$$

Note that this value is the same as $\binom{N-K}{M}$ divided by $\binom{N}{M}$, which is immediately understandable by viewing the selection as randomly choosing M cells out of N. The number of all, equally probable selections is $\binom{N}{M}$, and among them $\binom{N-K}{M}$ are FS aliquots.

Now we calculate FSL_{ap}, the FSL of the randomly chosen aliquot. Using that $FSL_{ap} = 1/(1 - q_a)$, $FSL_p = 1/p$ and $1 - p = (FSL_p - 1)/FSL_p$, from equation (1) we get

$$FSL_{ap} = \frac{FSL_p}{1 - \sum_{k=0}^{n-1} 2^{-k}(2 - 2^{-n})^{-1} q_{a|k}}. \tag{3}$$

Notice that the contribution of the terms $2^{-k}(2 - 2^{-n})^{-1} q_{a|k}$ in the summation of the above expression is negligible for large k. Therefore we get a good approximation for FSL_{ap} if we keep only the terms with $k < m$. In this case we can simplify expression (2) for $q_{a|k}$ by

$$(N - K) \times (N - K - 1) \times ... \times (N - M + 1)$$

to get

$$q_{a|k} = \tfrac{N-M}{N} \times \tfrac{N-M-1}{N-1} \times \tfrac{N-M-2}{N-2} \times ... \times \tfrac{N-M-K+1}{N-K+1} = \Pi_{j=0}^{K-1} \tfrac{N-M-j}{N-j}. \tag{4}$$

It is clear that

$$\tfrac{N-M-j}{N-j} < \tfrac{N-M}{N} = \tfrac{A-1}{A},$$

where $A = N/M$ is the number of aliquots generated from the pool of cells. Thus for $K := 2^k < M = 2^m$ we can approximate $q_{a|k}$ from above by

$$\left(\tfrac{A-1}{A}\right)^{2^k},$$

and from (3) we get the approximation

$$FSL_{ap} \approx \frac{FSL_p}{1 - \sum_{k=0}^{m-1} 2^{-k-1}(\frac{A-1}{A})^{2^k}}\,. \tag{5}$$

We note that this approximation is very good in practice for the range of M and N that we are using, when M is essentially smaller than N, which is more than a million.

Finally we calculate the ratio FSL_{ap}/FSL_a, called FSL drop, where FSL_a denotes the FSL of a separately produced pool with the same cell number M as that of the aliquot. By our observations, in the clinically relevant range, the logarithm of the FSL is approximately a linear function of the logarithm of the cell number of the pool, with slope close to minus one. This means, that in the clinically relevant range of cell numbers we have

$$\frac{FSL_p}{FSL_a} \approx \frac{M}{N} = \frac{1}{A}\,.$$

Consequently, from (5) we obtain

$$\frac{FSL_{ap}}{FSL_a} \approx \frac{1}{A\big(1 - \sum_{k=0}^{m-1} 2^{-k-1}(\frac{A-1}{A})^{2^k}\big)}\,. \tag{6}$$

The contribution of those terms of the sum in this formula, which correspond to large k, is very small. In other words, for large M only the first few terms (i.e. 15) of the sum should be considered, since the contribution of the other terms is negligible. This means, that practically the FSL drop depends only on the number of aliquots A, when the cell numbers of the aliquot and of the pool are sufficiently large. To make this argument more precise let d_m denote the right-hand side of (6) and estimate the error $\varepsilon_l = d_l - d_m$ that we make when we sum the terms until $l - 1 < m - 1$ in place of $m - 1$ in (6). Clearly, for any $l < m$ we have

$$\varepsilon_l = \frac{1}{A}\big((1-S_m)^{-1} - (1-S_l)^{-1}\big) \le \frac{S_m - S_l}{A(1-S_m)^2} < \frac{t_l}{A(1-S)^2}\,, \tag{7}$$

where for integers $j \ge 0$ we use the notations

$$S_j := \sum_{k=0}^{j} 2^{-k-1}(\tfrac{A-1}{A})^{2^k}, \quad S := \sum_{k=0}^{\infty} 2^{-k-1}(\tfrac{A-1}{A})^{2^k}, \quad t_j := \sum_{k=j+1}^{\infty} 2^{-k-1}(\tfrac{A-1}{A})^{2^k}.$$

Since $f(x) = 2^{-x}r^{-2^x}$ is a decreasing function of $x \in [0,\infty)$ for any $r \ge 1$, we get

$$t_l \le \frac{1}{2}\int_l^\infty 2^{-x}r^{-2^x}\,dx = \frac{1}{2\ln 2}\int_{2^l}^\infty y^{-2}r^{-y}\,dy \le \frac{2^{-2l}}{2\ln 2}\int_{2^l}^\infty r^{-y}\,dy = \frac{2^{-2l-1}}{\ln r \ln 2}r^{-2^l}, \tag{8}$$

with $r := A/(A-1)$. Notice that for every $j \ge 0$

$$1 - S \ge 1 - \sum_{k=0}^{j} 2^{-k-1} - t_j = 2^{-j-1} - 2^{-2j-1}(\ln r \ln 2)^{-1}r^{-2^j} = 2^{-j-1}(1 - 2^{-j}(\ln r \ln 2)^{-1}r^{-2^j}).$$

Thus choosing the smallest integer $j = j_0$ such that $j_0 \ge 1 - \log_2(\ln r \ln 2)$, we get

$$1 - S \ge 2^{-j_0-2} \ge 2^{-3}(\ln r \ln 2)$$

for all $A \ge 2$. Thus we have

$$(1-S)^2 \ge 2^{-6}(\ln r \ln 2)^2.$$

Using this together with estimate (8), from (7) we obtain

$$\varepsilon_l < \tfrac{1}{A(\ln 2 \ln r)^3} 2^{-2l+6} r^{-2^l}$$

for all $l \le m$ and $A \ge 2$, where $r = A/(A-1)$. Hence by the simple estimate

$$\ln r = \ln(1 + (A-1)^{-1}) \ge \ln 2 (A-1)^{-1},$$

valid for all $A \ge 2$, and since $(\ln 2)^{-6} < 10$, we get

$$\varepsilon_l < 10 \tfrac{(A-1)^3}{A} 2^{-2l+6} r^{-2^l} < 10 A^2 2^{-2l+6} r^{-2^l}.$$

Thus we can see that even for relatively large A, say $A = 512$, the error is negligible if $m > 15$ is replaced with 15 in the calculation of the FSL drop by the formula (6).